Departmental Papers (EES)   Department of Earth and Environmental Science

3-2013

Origin of Hysteresis in Bed Form Response to Unsteady Flows

Raleigh L. Martin
University of Pennsylvania

Douglas J. Jerolmack
University of Pennsylvania, sediment@sas.upenn.edu

Origin of Hysteresis in Bed Form Response to Unsteady Flows

Abstract

Field and laboratory studies indicate that changes in riverbed morphology often lag changes in water discharge. This lagged response produces hysteresis in the relationship between water discharge and bed form geometry. To understand these phenomena, we performed flume experiments to observe the response of a sand bed to step increases and decreases in water discharge. For an abrupt rise in discharge, we observed that bed forms grew rapidly by collision and merger of bed forms migrating with different celerities. Growth rate slowed as bed forms approached equilibrium with the higher discharge regime. After an abrupt discharge drop, bed form decay occurred through formation of smaller secondary bed forms, in equilibrium with the lower discharge, which cannibalized the original, relict features. We present a simple model framework to quantitatively predict time scales of bed form adjustment to flow changes, based on equilibrium bed form heights, lengths, and celerities at low and high flows. For rising discharge, the model assumes that all bed form collisions result in irreversible merger, due to a dispersion of initial celerities. For falling discharge, we derive a diffusion model for the decay of relict high-stage features. Our models predict the form and time scale of experimental bed form adjustments. Additional experiments applying slow and fast triangular flood waves show that bed form hysteresis occurs only when the time scale of flow change is faster than the modeled (and measured) bed form adjustment time. We show that our predicted adjustment time scales can also be used to predict the occurrence of bed form hysteresis in natural floods.

Disciplines
Earth Sciences | Environmental Sciences | Physical Sciences and Mathematics | Sedimentology | Water Resource Management

Origin of hysteresis in bed form response to unsteady flows

Raleigh L. Martin[1] and Douglas J. Jerolmack[1]

[1] Field and laboratory studies indicate that changes in riverbed morphology often lag changes in water discharge. This lagged response produces hysteresis in the relationship between water discharge and bed form geometry. To understand these phenomena, we performed flume experiments to observe the response of a sand bed to step increases and decreases in water discharge. For an abrupt rise in discharge, we observed that bed forms grew rapidly by collision and merger of bed forms migrating with different celerities. Growth rate slowed as bed forms approached equilibrium with the higher discharge regime. After an abrupt discharge drop, bed form decay occurred through formation of smaller secondary bed forms, in equilibrium with the lower discharge, which cannibalized the original, relict features. We present a simple model framework to quantitatively predict time scales of bed form adjustment to flow changes, based on equilibrium bed form heights, lengths, and celerities at low and high flows. For rising discharge, the model assumes that all bed form collisions result in irreversible merger, due to a dispersion of initial celerities. For falling discharge, we derive a diffusion model for the decay of relict high-stage features. Our models predict the form and time scale of experimental bed form adjustments. Additional experiments applying slow and fast triangular flood waves show that bed form hysteresis occurs only when the time scale of flow change is faster than the modeled (and measured) bed form adjustment time. We show that our predicted adjustment time scales can also be used to predict the occurrence of bed form hysteresis in natural floods.

1. Introduction

[2] Ripples and dunes commonly form in sand-bedded rivers under subcritical water flows [e.g., *Gilbert*, 1914; *Kennedy*, 1969; *Southard*, 1991]. Tracking the sizes and celerities of these "bed forms" is useful for computation of sediment flux [e.g., *Simons et al.*, 1965; *Bokuniewicz et al.*, 1977; *Nittrouer et al.*, 2008], stratigraphic reconstruction of past flows [e.g., *Jones* 1977; *Leclair* 2002; *Jerolmack and Mohrig*, 2005a; *Leclair and Blom*, 2005], determination of flow resistance [e.g., *Simons and Richardson*, 1961; *Wijbenga and Van Nes*, 1986; *Paarlberg et al.*, 2010], and prediction of solute transport rates [e.g., *Stonedahl et al.*, 2010; *Harvey et al.*, 2012]. Laboratory experiments and theory predict equilibrium relationships between bed form geometries and hydraulic conditions in steady flows [e.g., *Simons and Richardson*, 1961; *Yalin*, 1964; *Stein*, 1965; *Kennedy*, 1969; *Allen*, 1970; *Fredsoe*, 1982; *van Rijn*, 1984; *Yalin*, 1992; *Baas*, 1994; *Karim*, 1995; *Best*, 1996; *Karim*, 1999]. Application of these equilibrium relationships to rivers assumes "quasi-steadiness," meaning that bed form adjustments keep pace with flow changes. Literature indicates that such equilibrium relationships often poorly predict bed form dimensions in natural settings [e.g., *Neill*, 1968; *Allen*, 1976a; *Julien and Klaassen*, 1995; *Kostaschuk and Villard*, 1996; *Wewetzer and Duck*, 1999]. Part of the reason for disagreement between laboratory and field may be that bed forms do not adjust instantaneously to flow [e.g., *Allen*, 1973; *Gee*, 1975; *Wijbenga and Klaassen*, 1983; *Baas*, 1994; *Wilbers and Ten Brinke*, 2003], often leading to formation of hierarchies of bed forms of many sizes adjusted to a range of different flow conditions [*Allen*, 1968; *Neill*, 1968; *Coleman*, 1969; *Jones*, 1977; *Allen*, 1976a; *Bokuniewicz et al.*, 1977; *Rubin and McCulloch*, 1980; *Kostaschuk and Villard*, 1996; *Bartholoma et al.*, 2004; *Traykovski*, 2007]. In cases where discharge changes faster than bed forms can adjust, the quasi-steady assumption is violated, suggesting the need to consider transient as well as equilibrium dynamics in bed form models. This is particularly evident in observed cases of bed form hysteresis [*Allen*, 1974, 1976a; *Ten Brinke et al.*, 1999; *Julien et al.*, 2002; *Wilbers and Ten Brinke*, 2003; *Frings and Kleinhans*, 2008; *Paarlberg et al.*, 2010], where bed forms are larger on the flood falling limb than on the rising limb for equal discharges.

[3] Studies of transient bed form dynamics have largely focused on bed form growth from a flat bed under steady flow. Laboratory experiments indicate that ripples initiate at a wavelength proportional to grain diameter then grow through merger [*Coleman and Melville*, 1994, 1996] and predictable changes in planform morphology [*Baas et al.*,

[1]Department of Earth and Environmental Science, University of Pennsylvania, Philadelphia, Pennsylvania, USA.

Corresponding author: R. L. Martin, Department of Earth and Environmental Science, University of Pennsylvania, Philadelphia, PA 19104, USA. (raleighm@sas.upenn.edu)

1993; *Baas*, 1994; *Baas and De Koning*, 1995; *Baas*, 1999]. While sedimentologists typically classify ripples and dunes as hydrodynamically distinctive small and large bed features [e.g., *McLean*, 1990; *Southard*, 1991], observations of ripples steadily coarsening toward dune sizes without abrupt morphological changes suggest that "ripples" and "dunes" might simply refer to different stages of bed form growth on the path to equilibrium [*Raudkivi*, 2006; *Fourriere et al.*, 2010; *Charru et al.*, 2013]. Numerical studies of bed form initiation and growth support the notion of a continuous process of bed form merger toward equilibrium [*Nikora and Hicks*, 1997; *Nino et al.*, 2002; *Jerolmack and Mohrig*, 2005b; *Paarlberg et al.*, 2009, 2010]. Given the uncertainty of the ripple/dune distinction, and, to our knowledge, no physical demonstration of a distinct phase transition between ripples and dunes, we choose simply to adopt the term "bed form" from here onward.

[4] Only a few experiments have considered the response of existing bed forms (rather than a flat bed) to changes in flow. *Gee* [1975] performed experiments tracking bed form response to step increases and decreases in discharge and found that the time scale of bed form adjustment is determined by the rate of sediment transport relative to the necessary volume of sediment to be displaced. Several researchers [*Bagnold*, 1941; *Allen*, 1974; *Allen and Friend*, 1976; *Lancaster*, 1988; *Rubin and Ikeda*, 1990] have adopted the notion of a bed form "reconstitution time," T^r, to describe how bed forms respond to changes in flow based on their sizes. Here, we adopt a specific definition for T^r:

$$T^r = \frac{V}{q_s}, \qquad (1)$$

where V is the minimum volumetric sediment displacement for the bed form adjustment (the "reconstitution volume") and q_s is sediment flux. According to this definition, *Gee* [1975] found that, relative to T^r, bed form growth took significantly longer than decay. He ascribed this difference to the greater "efficiency" of the decay process but did not explain the origin of this efficiency. Similar step-change experiments performed by *Wijbenga and Klaassen* [1983] confirmed this finding. *Wijbenga and Van Nes* [1986] tracked bed form changes through sinusoidal and natural flood waves reproduced in a laboratory flume. They observed hysteresis in bed form lengths, heights, and flow resistance relative to changes in discharge, and shorter floods showed more pronounced lags and hysteresis, though bed form heights tended to adjust more quickly than lengths. Step change experiments by *Nelson et al.*, [2011] and field observations by *Wilbers and Ten Brinke* [2003] also noted the faster adjustment of bed form heights versus lengths.

[5] Theoretical, empirical, and numerical models of bed form growth adjustment have been proposed. *Allen* [1976b, 1976c, 1976d] and *Fredsoe* [1979] made theoretical predictions for bed form adjustment based on the rates at which individual bed forms persist as coherent forms (related to T^r) and the rates at which these coherent forms change their dimensions over time. However, experimental [*Wijbenga and Klaassen* 1983] and field [*Gabel* 1993] observations disagreed substantially with their theories. *Baas* [1994, 1999] determined experimentally that bed forms grow toward steady state over a time scale proportional to an empirically fit inverse power of flow velocity, though his prediction is based only on a fit to data and lacks a physical mechanism underlying the predicted time scale. Numerical models successfully describing bed form growth to equilibrium have been built based on statistical and rules-based descriptions of crestline merger due to varying bed form celerities [*Fuhrboter*, 1983; *Raudkivi and Witte*, 1990; *Nikora and Hicks*, 1997; *Betat et al.*, 1999; *Flemming*, 2000], annihilation and reorientation of defects in planform bed configurations [*Werner and Kocurek*, 1997, 1999; *Huntley et al.*, 2008; *Kocurek et al.*, 2010], discrete element modeling [*Nino et al.* 2002], continuum treatment of bed form adjustment as a diffusion process [*Jerolmack and Mohrig*, 2005b], and direct numerical modeling of coupled flow and transport equations [*Paarlberg et al.*, 2009; *Shimizu et al.*, 2009; *Paarlberg et al.*, 2010; *Nelson et al.*, 2011]. However, none of these models offer a simple, physically based predictive framework for determining bed form adjustment time.

[6] No quantitative predictions exist for the time scale of bed form decay following a reduction in discharge. Field observations by *Wilbers and Ten Brinke* [2003] indicate that a drop in water discharge induces the formation of small, secondary bed forms on the stoss sides of larger forms generated up to the flood peak. These secondary forms gradually reduce dimensions of the bed form field by cannibalizing relict flood peak bed topography. While the time lag in destruction of relict large bed forms has been invoked to model hierarchies of bed form dimensions in unsteady flow fields [*Allen*, 1968; *Jones*, 1977; *Nikora et al.*, 1997], no quantitative theory has been tested experimentally to predict the time scale of bed form decay in response to a reduction in discharge.

[7] In this article, we describe flume experiments to observe the form and time scale of sand bed form adjustment to flow increases and decreases of varying magnitude. We begin by describing in detail the evolution of bed topography following both step flow changes and artificially produced triangular flood waves. We propose simple but distinctive models for bed form growth and decay, which predict adjustment rates in terms of bed form reconstitution time. We then show how, in our experiments, bed form hysteresis arises when discharges change more quickly than predicted bed form adjustment time scales. Finally, we show how our theory can be applied to predict the occurrence of bed form hysteresis in natural flood waves, and we discuss implications for river hydraulics, stratigraphy, stream ecology, and flow nonuniformity.

2. Experiments

[8] Experiments were conducted during the summer of 2011 on the "Tilting Bed Flume" at the Saint Anthony Falls Laboratory (SAFL) at the University of Minnesota in Minneapolis, MN (Figure 1a). The flume is a rectangular channel with length, width, and depth of 15.0, 0.92, and 0.65 m, respectively, and the bed of the flume structure was adjusted to zero slope. Water discharge was controlled manually by a hydraulically actuated valve, and flow rates were determined by a linear calibration curve. Water, which was fed directly from the adjacent Mississippi River, entered the flume through a large pipe submerged in an

upstream head box and exited the flume over a 26 cm high tailgate, which maintained a minimum flow depth within the flume to prevent the formation of lateral instabilities and braiding. A sediment recirculation pump (described below) drew its water directly from the head box of the flume; thus, it did not add to the overall flume discharge. Due to uncertainties in the calibration curve and head variations in the inlet water source, uncertainty in reported discharge values is about ±4%.

[9] The flume contained a roughly constant volume of sand, which was retained in the flume by a recirculating pump. Sand size distribution, measured using a Retsch Camsizer, was roughly lognormal, with median diameter,

$D_{50} = 0.37$ mm, and range $D_{10} = 0.25$ mm to $D_{90} = 0.58$ mm, representing the 10th and 90th percentiles of grain size, respectively. Measured sand density was $\rho_s = 2.60$ g/mL, and measured surface bed sediment volume fraction was $\varphi = 0.58$. Downstream of the test section, a 20 cm wall maintained a minimum depth of sediment in the flume, so that bed forms would never scour down to the flume bed. (With the 26 cm tailgate, minimum water depth in the flume was thus 6 cm.) Downstream sand flux spilling over the wall settled into a submerged funnel located roughly 14 m downstream of the head box. After settling to the bottom, a water jet carried the sediment back to the upstream end of the flume, releasing it evenly across the channel cross-section. Immediately prior to shutting off the flume for some of the experiments, we directly measured sediment flux by stopping the recirculation funnel and collecting sediment over a defined period of time longer than the mean time of bed form passage. Total sediment fluxes measured by this method at $Q = 39.1$, 63.3, 81.1, and 111.7 L/s, were $q_s = 0.0044$, 0.020, 0.20, and 0.77 cm^2/s, respectively. Total sediment fluxes ranged across orders of magnitude, rising approximately as the fifth power of discharge.

[10] Flume inlet and outlet conditions introduced some nonuniformity in flow conditions, which we tried to minimize in the experimental setup and analysis. Flow dissipating structures, including a mesh of cobbles and a matrix of upright plastic pipes, helped to straighten and smooth the water flow from the head box. Nonetheless, a zone of sediment scour formed downstream of the flow straightener, extending to about 3 m from the head box. Usage of a tailgate to maintain a minimum flow depth also introduced a backwater effect that extended across the entire flume
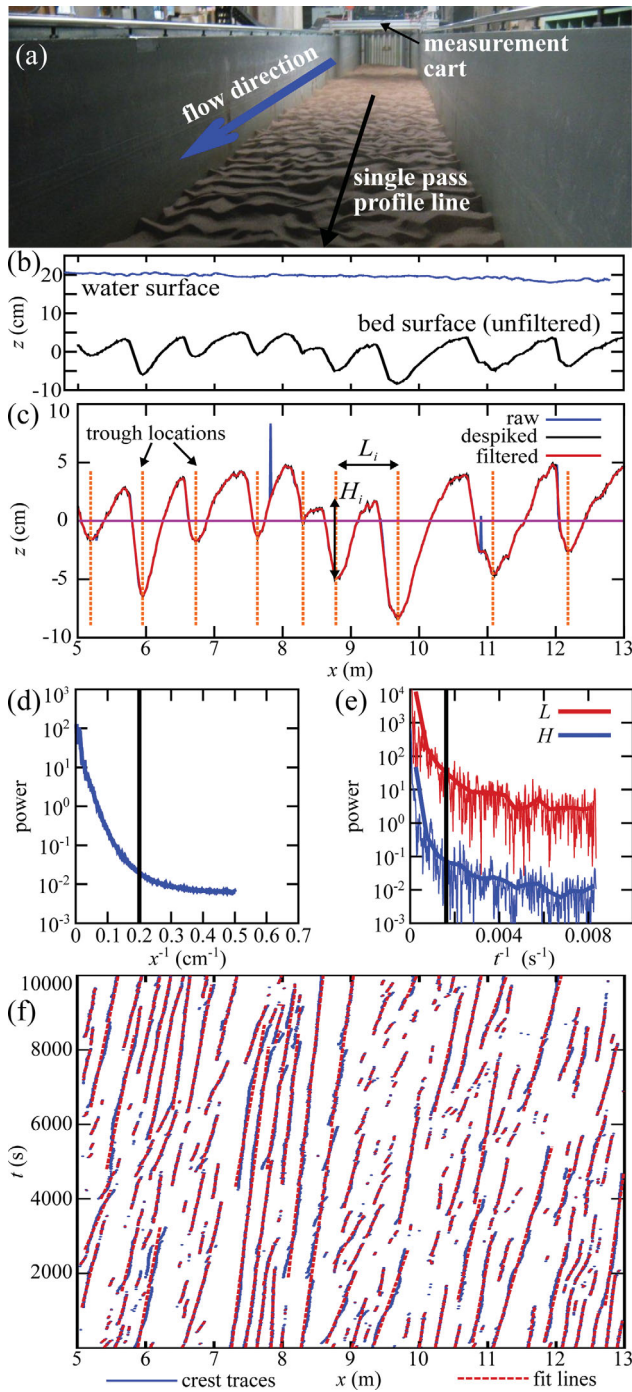

Figure 1. (a) View of flume looking upstream, showing bed forms formed at 39.1 L/s. Sonar and ultrasonic probe connected to the measurement cart obtained longitudinal profiles of water surface and bed elevation, z. (b) An example of water surface and bed elevation profiles is shown for $t = 20,000$ s in experiment S2. (c) Lengths of individual bed forms (L_i) were measured as distances between successive troughs. Heights (H_i) were measured as elevation changes from troughs to nearest downstream crests. Trough and crest locations were determined as minima and maxima, respectively, between zero-crossings, where "0" was defined as mean bed elevation. To eliminate spurious zero-crossings prior to calculation of bed form dimensions, raw profiles (blue) were processed to remove anomalous spikes (black), and a moving-average spatial filter was applied to remove high-frequency noise (red). (d) Power spectra of bed elevation (here shown as the ensemble average of spectra over all bed profiles for experiment S2) were used to determine a white noise threshold of $x = 5$ cm (black line) used for the moving average filter. (e) Power spectra of bed form length (red) and height (blue) time series in experiment S2 illustrate choice of a 600 s time-averaging window (black line) for calculating bed form geometry statistics. In this plot, thin lines are raw power spectra and thick lines are moving averages. (f) Crest locations (blue) and crestline fit lines (red dashed) for a 10,000 s interval at the beginning of experiment S2. Slopes of fit lines were used to determine bed form celerities.

Table 1. Summary of Initial (Q_{1a}), Peak (Q_2), and Final (Q_{1b}) Equilibria for Step-Discharge Change Experiments[a]

Run	Q_{1a} (L/s)	h_{1a} (cm)	S_{1a} (%)	τ_{1a}^*	P_{1a}	H_{1a} (cm)	L_{1a} (cm)	H_{1a}/L_{1a}	β_{1a}	k_{1a}^L	c_{1a} (cm/s)	$q_{s,1a}^t$ (cm²/s)
						Initial Low Flow (Q_{1a})						
S1	39.1	12.9	0.110	0.15	1.8	3.2	65.9	0.060	0.54	2.8	0.032	0.030
S2	39.1	13.8	0.103	0.15	1.8	2.2	34.7	0.072	0.51	3.8	0.014	0.009
S3	39.1	15.3	0.083	0.13	1.9	2.3	35.6	0.075	0.51	3.6	0.010	0.007
D1	63.3	18.1	0.100	0.19	1.6	2.6	44.8	0.066	0.51	3.3	0.033	0.025
D2	63.3	18.0	0.111	0.20	1.5	2.7	45.3	0.068	0.52	3.6	0.034	0.027
						High Flow (Q_2)						
S1	111.7	21.9	0.337	0.76	0.8	7.8	130.2	0.065	0.53	6.3	0.129	0.292
S2	81.4	19.7	0.176	0.36	1.2	6.2	90.7	0.072	0.54	8.5	0.069	0.124
S3	81.4	20.4	0.145	0.30	1.3	5.0	79.3	0.061	0.54	4.1	0.084	0.122
D1	81.4	20.4	0.133	0.28	1.3	4.3	70.9	0.062	0.53	4.5	0.043	0.054
D2	111.7	23.7	0.219	0.53	1.0	6.7	107.4	0.066	0.52	4.7	0.072	0.140
						Final Low Flow (Q_{1b})						
S1	39.1	14.5	0.103	0.15	1.8	2.5	49.5	0.062	0.48	2.3	0.021	0.015
S2	39.1	14.7	0.087	0.13	1.9	2.4	38.5	0.070	0.49	3.4	0.014	0.009
S3	39.1	15.6	0.070	0.11	2.1	2.4	39.3	0.069	0.51	4.2	0.010	0.007
D1	63.3	18.0	0.100	0.18	1.6	2.6	48.0	0.063	0.50	3.1	0.035	0.026
D2	63.3	18.5	0.101	0.19	1.6	3.0	51.4	0.068	0.52	3.0	0.030	0.026

[a]Equilibria were calculated from the last 7200 s (2 h) of each flow condition for step-discharge experiments. Q is water discharge, h is flow depth, S is water surface slope, τ^* is Shields stress, P is Rouse number, H is mean bed form height, L is mean bed form length, H/L is bed form steepness, β is bed form shape parameter, k^L is gamma parameter for bed form lengths, c is mean bed form celerity, and q_s^t is translation sediment flux. Subscripts refer to the segment of the experiment (1a for initial low flow, 2 for high flow, and 1b for final low flow).

length. Given these inlet and outlet conditions, we limited our bed form analyses to the zone from 5 to 13 m downstream of the flume head box, across which we found flow depth and water surface slope to be roughly uniform.

[11] We carried out a series of experiments consisting of step changes between a low (Q_1) and a high (Q_2) discharge. As summarized in Table 1, five different experiments were performed for different relative discharge changes. The step changes were made by manually adjusting the intake valve pressure at appointed times. In each of these experiments, we first allowed bed forms to develop to a steady state at Q_1. Then, we abruptly increased discharge to Q_2, allowing bed forms to grow and then achieve a new equilibrium. After several hours of steady-state bed form migration at Q_2, we reduced discharge back to Q_1, allowed bed forms to decay, and continued to observe steady state bed form migration for several hours. Unlike the step adjustment experiments of *Gee* [1975] and *Wijbenga and Klaassen* [1983], which utilized feedback controls to maintain constant energy slopes in their flumes, the imposed tailgate backwater condition in our experiment caused both water surface slope and flow depth to change in response to discharge changes.

[12] In addition to the step discharge experiments, we performed two additional experiments, in which we gradually increased discharge from $Q_1 = 39.1$ L/s to $Q_2 = 111.7$ L/s, then gradually decreased discharge back to Q_1, approximating triangular flood waves. In the "slow" experiment, the total duration of the wave (rise and fall) was 8 h, while in the "fast" experiment, the duration was 2 h. Operationally, the discharge change was achieved by incremental manual adjustments of discharge at regular intervals (20 and 5 min for slow and fast flood waves, respectively).

[13] We measured bed topography during experiments by successive sonar scans using a JSR Ultrasonic DPR300 Pulser/Receiver. The sonar arm, which was minimally submerged about 1 cm below the water surface (to reduce

flow disturbances), swept up and down the length of the observation section along longitudinal transect(s), recording bed elevation at 1 cm intervals. The sonar recorded bed topography with submillimeter resolution, though uncertainty in picking out the sonar waveform peak suggests vertical accuracy on the order of 1 mm. Water surface elevation was simultaneously captured by a MassaSonic M-5000/220 ultrasonic probe attached on the track with the sonar, also with 1 cm horizontal resolution and vertical resolution of 0.25 mm. The sonar and ultrasonic probe together took about 10 s to traverse each transect. Based on the short duration of the sonar pass relative to bed form celerities, we assume that each sonar pass provided an instantaneous representation of bed state.

[14] Three step change experiments (the "S" single pass experiments in Table 1) consisted of a single transect down the flume centerline, measuring a complete bed profile at approximately 18 s intervals. Bed topography in the triangular flood wave experiments was also measured via single pass sonar transects. For the two other step change experiments (the "D" double pass experiments in Table 1), we captured two parallel transects, equidistant from the flume centerline and spaced apart by a transverse distance of 30 cm. The time interval for each pair of parallel transects was about 38 s. The single pass versus double pass experiments offered a trade-off in spatial versus temporal resolution. After a few of the experiments, we carefully drained the flume to reveal a field of bed forms (Figure 1a), then captured high-resolution maps of bed topography using a Keyence LKG502 laser scanner. These laser scans revealed no significant difference between the centerline and parallel passes, thus we treat the single and double pass results as equivalent.

3. Data Processing

[15] Measurement scans produced concurrent profiles of water and bed-surface elevations (Figure 1b), which

required data filtering (Figure 1c). First, spurious peaks in bed-surface profiles, caused by localized sediment suspension events, were "despiked" by interpolating over positions where measured bed slope exceeded ± 0.5 ($\pm 26.6°$). A similar processing was carried out by *Coleman and Melville* [1994]. Second, a "zero-line" was established for bed profiles by subtracting the mean elevation from each profile. We considered detrending data by global sand bed slope; however, due to the presence of the bed forms, it would have been difficult to determine a consistent detrending slope, so we adopted the assumption of a flat sand bed. Given the presence of a backwater effect, the bed slope was very small (as in downstream reaches of rivers [e.g., *Nittrouer et al.*, 2012]), and elevation change due to reach-scale slope was negligible compared to the height of individual bed forms. Third, a 5 cm triangular moving average filter was applied to bed profiles to eliminate high frequency noise that might have disrupted the zero-crossing method. The length of moving average window was chosen based on ensemble-averaged power spectra of bed-elevation profiles (Figure 1d), which indicated a 5 cm cutoff for the spectral white noise regime.

[16] We performed data processing techniques similar to past work [*Nordin*, 1971; *van der Mark and Blom*, 2007; *van der Mark et al.*, 2008] to determine bed form dimensions. First, locations of zero-crossings were identified for the filtered bed profiles. Crests were determined as maxima and minima between successive zero-crossings (Figure 1c). We defined individual bed forms to span the distance between two successive troughs. Individual bed form lengths, L_i, were calculated from intertrough distances, while individual heights, H_i, were determined as elevation changes from troughs to downstream crests. Individual bed form steepnesses were determined as the ratio of H_i/L_i, while bed form shape factor, β_i, was determined as $\beta_i = A_i/(H_iL_i)$, where A_i is the total area of sediment above the minimum bed form elevation. (Here and subsequently, the "i" subscript indicates that a variable is for an individual bed form; otherwise, variables refer to mean quantities.)

[17] Bed form geometries displayed large variability; so, we estimated mean bed form dimensions based on temporal and spatial averaging. We divided bed form geometry time series into 600 s windows and calculated mean H, L, H/L, and β based on means of all bed forms observed over these time windows. Just as we did for the spatial moving average, we computed power spectra of H and L time series (Figure 1e) to justify choice of this temporal cutoff. All subsequently described bed form time series are based on these 600 s window computations.

[18] We determined bed form celerities, c, by tracking crestlines [e.g., *Coleman and Melville*, 1994]. First, we generated space-time plots of crest positions (Figure 1f). Then, across individual time steps, we considered crests within $\pm L_{min} = 8.3$ cm to be the same continuous crestline feature. L_{min} was chosen as our minimum bed form length based on experimental median grain size (here, $D_{50} = 0.37$ mm) and an empirical relation for lengths of new bed forms generated by flat bed instabilities [$L_{min} = 175D_{50}^{0.75}$; equation (3), *Coleman and Eling*, 2000]. We assumed that successive crest positions spanning a distance less than L_{min} could not be distinctive forms. We then fit lines to individual crestlines (shown as red dashed lines in Figure 1f) and

determined crestline celerities based on the slopes of these lines. Weighting the collection of measured celerities by crestline track lengths, we determined the means and distributions of bed form celerities over 600 s windows for comparison with other bed form parameters.

[19] As described earlier, we directly measured sediment fluxes at the end of a few experiments. However, we could not directly measure sediment flux time series during the experiments. Thus, we estimated sediment flux based on the celerities and sizes of bed forms [e.g., *Simons et al.*, 1965]. We computed this "translation" sediment flux, q_s^t, as:

$$q_s^t = \beta\phi cH. \tag{2}$$

q_s^t does not represent the total sediment flux; it only measures that component of flux contributing to bed form migration. As described by *McElroy and Mohrig* [2009], q_s^t roughly accounts for bed load while neglecting suspended load.

[20] Finally, we calculated flow depths, h, based on differences between water surface and bed elevations, and we calculated water surface slopes, S, based on linear fits to water surface elevation profiles. For consistency, the 600 s window averaging was also applied to measurements of h and S.

[21] While we tried to reproduce similar hydraulic conditions for multiple experiments, unavoidable differences arose among different runs. Part of this was due to uncertainty of manually adjusted water discharge. Furthermore, suspension of sediment, especially at higher discharges (for lower Rouse numbers, P), caused some sand to be lost from the flume, changing the overall depth of sediment to the flume bed and also affecting water surface slope and flow depth. Nonetheless, each step discharge change presented its own set beginning, peak, and ending equilibrium conditions, henceforth denoted with subscripts of "$1a$," "2," and "$1b$," respectively, for specific experimental segments. For each step experiment, we estimated equilibrium hydraulic and bed form quantities (i.e., H_{1a}, H_2, H_{1b}, L_{1a}, etc.) by averaging over the 600 s window-averaged time series (i.e., H, L, etc.) in the final 2 h (7200 s) of each discharge segment of each experiment. The resulting equilibrium values are provided in Table 1.

4. Observations of Transient Bed-Form Evolution

[22] We begin our data analysis by considering an individual step discharge experiment, S2, with a low discharge of $Q_1 = 39.1$ L/s and a high discharge of $Q_2 = 81.4$ L/s. We describe S2 here as a representative example; the other step discharge experiments displayed similar processes. In describing this and other experiments, t is the absolute time from the beginning of the experiment, while t_{12} and t_{21} are the relative times from the onset of the "rising" $Q_1 \rightarrow Q_2$ and "falling" $Q_2 \rightarrow Q_1$ transitions, respectively.

4.1. Bed-Form Growth Observations

[23] Figure 2 shows time series of calculated the 600 s window-averaged quantities describing hydraulic and bed form development through the S2 experiment. The increase in water discharge, Q, caused abrupt increases in both flow

depth, h, and water surface slope, S. Compared to these abrupt hydraulic changes, bed form heights, H, and lengths, L, increased gradually over a period of about 5000 sec. Bed form steepness, H/L, remained roughly constant (≈ 0.07);
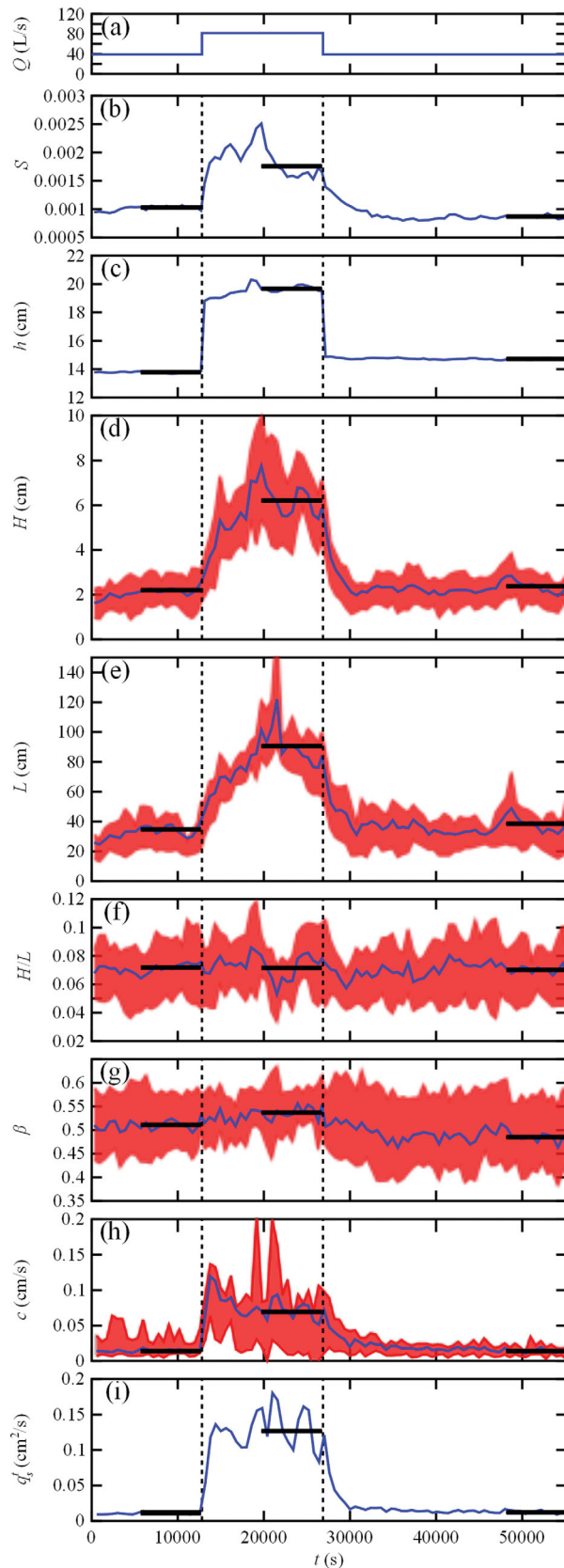
thus, bed form growth was equally accommodated by changes in H and L. Shape factor, β, increased slightly, though by a small amount relative to the measured variability around the long-run mean of $\beta \approx 0.5$. Celerities, c, increased abruptly then gradually declined to a new equilibrium, c_2, which was higher than the initial c_1. Translation sediment flux, q_s^t, calculated here and throughout the paper assuming $\beta = 0.5$ in equation (2), also increased abruptly but then maintained a constant equilibrium value, $q_{s,2}^t$. Simultaneous increase in H and decrease in c through the transition account for this constant q_s^t. Throughout the rising transition (and the entire experimental run), bed form parameters showed a large degree of variability among individual forms, as indicated by the red shaded areas in Figure 2.

[24] Figure 3 qualitatively exhibits the bed form growth process. In Figure 3a, a space-time plot of bed elevation shows bed form heights and lengths growing with increasing time, t_{12}, from the rising transition. Figure 3b, which illustrates a "color map" of bed elevations along axes of space and time, displays continuous traces of forward migrating bed forms. As t_{12} increases, the heights and lengths of individual bed forms increase, while the number of crestline traces decreases. Leftward bending of bed form traces in the color map indicates decline in c with increasing t_{12}. Together, these plots indicate that bed form growth is accomplished through the merger of many small, fast-migrating bed forms into fewer, larger, slower-migrating bed forms.

[25] Zoomed-in subsets of the space-time and color map plots shown in Figure 4 detail bed form interactions in the growth process. In Figure 4a, manually traced crestlines of individual migrating bed forms show that bed form celerities vary, causing them to collide and interact. In some cases, such as illustrated at $t_{12} \approx 2500$ s, two colliding bed forms merge, creating a new, larger bed form. The increased color contrast at the site of bed form collision in the color map (Figure 4b) indicates the increased size of the new merged bed form. Bed form collision may also result in a "pass-through" interaction, such as illustrated at $t_{12} \approx 4000$ s. Here, a trailing small bed form approaches a slower, larger leading bed form. Following the interaction, mass is transferred from the leading to the trailing form, making it appear as if the small form is passing through the larger one. This pass-through interaction allows bed forms to continue interacting in steady state while maintaining equilibrium geometries. Merger

Figure 2. Experiment S2: time series of (a) water discharge, Q, (b) water surface slope, S, (c) flow depth, h, (d) bed form height, H, (e) bed form length, L, (f) steepness, H/L, (g) shape factor, β, (h) celerity, c, and (i) translation sediment flux, q_s^t. Mean time series values (blue) are based on 600 s window averages, while the red areas indicate the middle 25th−75th percentile range for bed form dimensions and celerities (d−h). Vertical dashed lines correspond to times of discharge changes shown in Figure 1a. Horizontal black lines show estimates of equilibrium values calculated over 2 h windows indicated by the ranges of the lines. These values are also listed in Table 1.
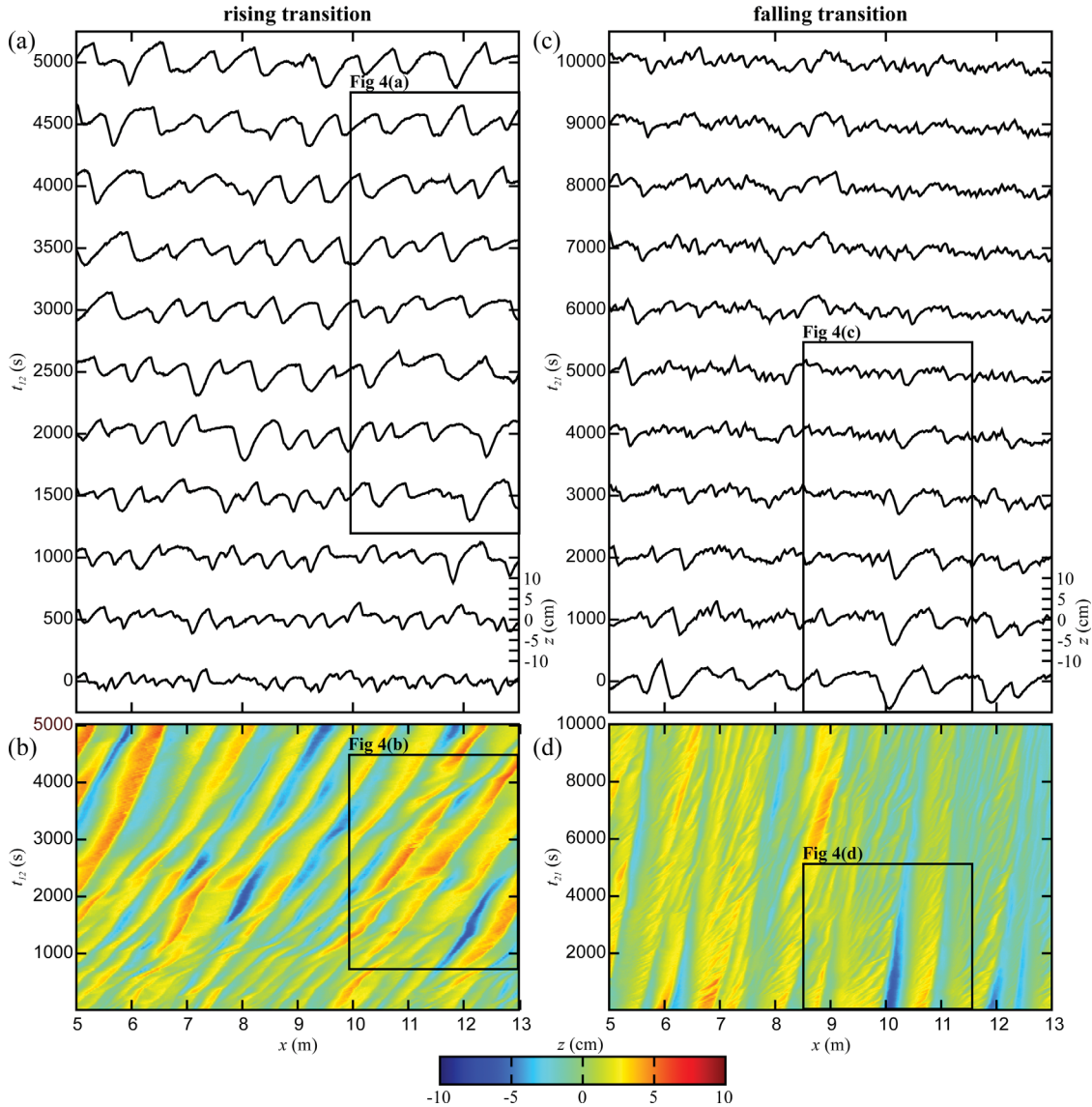
Figure 3. Visualization of rising (a, b) and falling (c, d) bed form transitions for experiment S2. Figures 3a and 3c show successive longitudinal bed profiles through time (increasing in the positive y-direction). The scale of the bed form profiles is shown on the bottom right of each plot. Figures 3b and 3d show color maps of bed elevation. t_{12} and t_{21} are the times from rising and falling discharge transitions, respectively. Rising transition plots show bed form growth by merger, while falling transition plots show bed form decay by formation of secondary bed forms, which cannibalize relict features. Detailed dynamics of transition processes are shown in Figure 4 for the outlined subset boxes.

and pass-through interactions were directly observed experimentally [e.g., *Endo et al.*, 2004] and in time-lapse images of aeolian dunes [e.g., *Vermeesch*, 2011], and these interactions have been used to explain the process of aeolian dune field construction [e.g., *Schwammle and Herrmann*, 2003; *Katsuki et al.*, 2005; *Kocurek et al.*, 2010].

4.2. Bed-Form Decay Observations

[26] As shown in Figure 2, when discharge decreased from Q_2 back to Q_1 in the falling transition, h decreased abruptly while S decreased gradually over a span of about 5000 s. H and L decreased over the same 5000 s span corre-

sponding to the S decline. The concurrent decreases in S, H, and L indicate a gradual decline in surface friction as shrinking bed forms exert progressively smaller form drag on the water flow. H/L remained roughly constant (as in the rising transition), while β decreased slightly but insignificantly compared with β variability. c and q_s^t also declined gradually over a 5000 s span following the discharge reduction, though, as we explain below, these gradual declines may be misleading artifacts of the data processing method.

[27] Figures 3c and 3d show space-time and color map plots of bed form adjustment versus time, t_{21}, from the step discharge reduction. Immediately following the Q drop, small, secondary bed forms develop on the stoss sides of
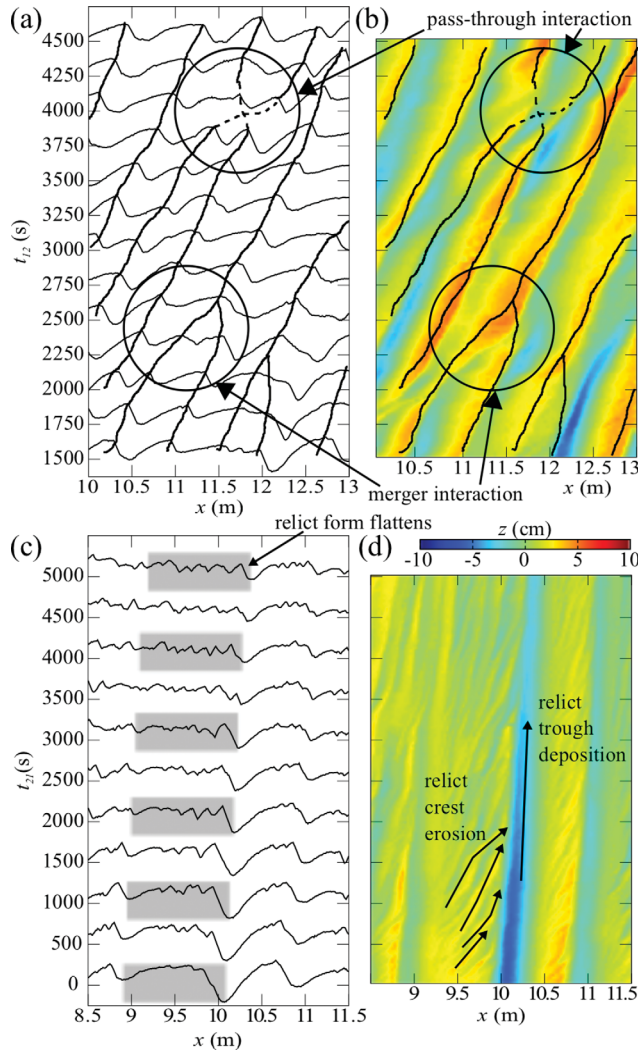
Figure 4. Subset plots of Figure 3 showing bed form interactions contributing to bed form growth and decay. In Figures 4a and 4b, crestlines have been traced, showing a merger occurring at $t_{12} \approx 2500$ s and a pass-through interaction at $t_{12} \approx 4000$ s. The merger interaction results in bed form heightening, while the pass-through interaction is indicated by mass transfer from the downstream to the upstream bed form. In Figure 4c, a large relict bed form, outlined in gray, is shown to gradually decay through time with the formation and migration of secondary bed forms. This is particularly apparent in Figure 4d, where migrating secondary bed forms erode the relict crest and deposit sediment in the relict trough. This process of relict bed form flattening suggests that bed form decay occurs as a diffusion process.

the larger forms created at high discharge. As can be seen in Figure 3d, secondary bed forms migrate rapidly, while the primary, relict forms move very slowly. Gradually, the relict forms shrink in size, while the secondary forms dominate the bed profile by about 5000 s.

[28] The subset plots in Figure 4 illustrate the specific bed form interactions producing the gradual declines in H and L. The gray boxes in Figure 4c show the area of one relict bed form, which flattens with growing t_{21} due to the increasing development of secondary bed forms. In Figure 4d, the indi-

vidual secondary bed form traces can be seen migrating over the edge of the relict form. As they do, they erode mass from the relict crest and deposit it in the relict trough, while also advancing the relict bed form very slowly. The secondary bed forms effectively act as an agent of diffusion, gradually reducing the elevation gradient between relict crests and troughs.

[29] We noted above a gradual decline in c and q_s^t with t_{21}; however, these observations may be strongly related to the zero-crossing method for locating bed form crestlines and celerities. Many of the secondary bed forms created immediately following the Q drop do not get captured by the zero-crossing method, because they are entirely contained above the zero line. Thus, the H and L measurements mostly describe the sizes of large, relict bed forms. In contrast, celerities determined from crestline velocities mostly record the c of secondary bed forms, since the majority of migrating crestlines (including those captured by the zero-crossing method) are those of fast-migrating secondary forms. The c time series indicates a gradual decline in secondary bed form celerities associated with the growth and slowing of these secondary bed forms. However, the q_s^t time series predicts unreasonably large sediment fluxes based on multiplying secondary bed form celerities with relict bed form heights. We did observe that local regions of fast, shallow flow (presumably caused by flow acceleration over relict crestlines) produced locally high sediment fluxes immediately following the Q drop. However, we believe that the measured slow decline in q_s^t is unrealistic. We expect that, following the step discharge drop, translation flux of secondary bed forms actually dropped quickly to its low flow equilibrium value, $q_{s,1}^t$.

4.3. Flood Wave Observations

[30] In contrast to the step discharge adjustments described thus far, we now consider bed form response to gradually varying discharges more representative of natural flood waves. Figure 5 shows how discharge varied with time for the experimental slow and fast waves, respectively. The steps in the plot show how we manually increased and decreased discharge in small increments to produce the triangular flood waves. Below the Q curves, plots of bed form heights and lengths show the differing bed-orm responses for the two experiments. Whereas H and L responded mostly in phase to the slow flood wave Q changes, H and L substantially lagged Q changes in the fast flood wave. In addition, H and L achieved higher peak values in the fast wave compared to the slow wave. The oscillatory nature of L during the Q decline in the slow wave is somewhat inexplicable; it may be related to the method of manual incremental changes in Q, though the effect does not arise for H.

[31] The differences between bed form responses to slow and fast flood waves are particularly striking in Figure 6. Here, H and L are plotted versus Q over the durations of the flood waves, and observations from flood rising and falling limbs are distinguished by upward and downward facing triangles, respectively. Both the slow and fast experiments show that H and L were higher on the falling limb than on the rising limb; however, the magnitude of this hysteresis was substantially greater through the fast flood wave. Furthermore, H and L continued to increase
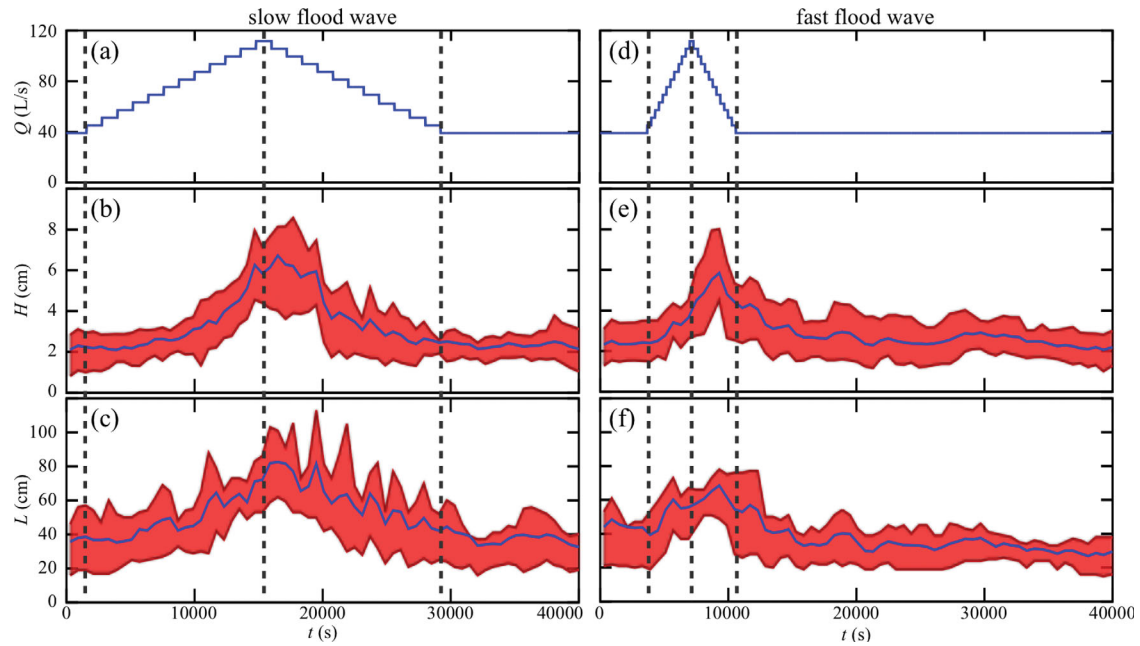
Figure 5. Bed form development for experimental flood waves. Plots of water discharge, Q, bed form height, H, and bed form length, L, are shown for the slow flood wave in Figures 5a–5c and for the fast flood wave in Figures 5d–5f. Blue curves describe average values, while red areas give 25th to 75th percentile ranges. In both experiments, H and L lag Q, though these lags are more pronounced in the fast flood wave, where H and L are substantially out of phase with discharge changes. Also, for the fast flood wave, bed form decay continues well beyond the time when discharge has subsided.

after the peak Q in the fast wave, while this did not occur in the slow wave. Except for the slight hysteresis, slow flood wave bed forms effectively maintained quasi-steady equilibrium with Q, which was clearly not the case for the fast flood wave. In particular, much of the decline in fast wave H and L occurred only after Q had already decreased to its minimum value of Q_1. The slight drop in rising limb L when $Q \approx 80$ L/s may be related to a morphological transition from ripples to dunes [*Robert and Uhlman*, 2001], though it likely results from the large variability in sampled bed forms.

5. Bed-Form Adjustment Time Scales

[32] In Figure 7, we offer a conceptual diagram summarizing the observations of bed form merger growth and cannibalization decay. In Figure 7a, small bed forms, with a mixture of sizes, move with celerities inversely proportional to their heights. When a smaller bed form approaches a larger one, they merge. By this process of merger, bed forms grow in height and length. In Figure 7b, small bed forms appear on the stoss slope of a large relict bed form, and these small bed forms erode the relict crest and fill the relict trough, until the relict bed form has been eliminated.

[33] Based on these qualitative observations of adjustment processes, below we consider quantitatively how time scales of bed form adjustments depend on reconstitution time scales for the bed form growth and decay processes. We then normalize experimental times by these reconstitution time scales to demonstrate the similar adjustment pro-

cess occurring for all of the step discharge change experiments.

5.1. Bed-Form Reconstitution Time Scales

[34] Adapting equation (1), we define specific bed form reconstitution times, T_{12}^r and T_{21}^r, for growth and decay adjustments, respectively, based on the reconstitution volumes versus the displacing sediment fluxes:

$$T_{12}^r = \frac{V_1}{q_{s,2}^t}, \tag{3}$$

$$T_{21}^r = \frac{V_2}{q_{s,1}^t}. \tag{4}$$

V_1 and V_2 are the low and high flow reconstitution volumes, and $q_{s,1}^t$ and $q_{s,2}^t$ are low and high translation sediment fluxes, respectively. Here, we express volumes and sediment fluxes per unit width, i.e., with dimensions of L^3/L and $L^3/T/L$, respectively. In calculating bed form reconstitution times, we assume that translation flux, q_s^t, dominates bed form adjustment.

[35] We quantify bed form reconstitution volumes and sediment fluxes in terms of equilibrium bed form heights, lengths, and celerities. We estimate V_1 as the mean volume of initial small (Q_1) equilibrium bed forms covering the length, L_2, of a single large mean equilibrium Q_2 bed form (Figure 7a). Conversely, V_2 is the volume of a single large
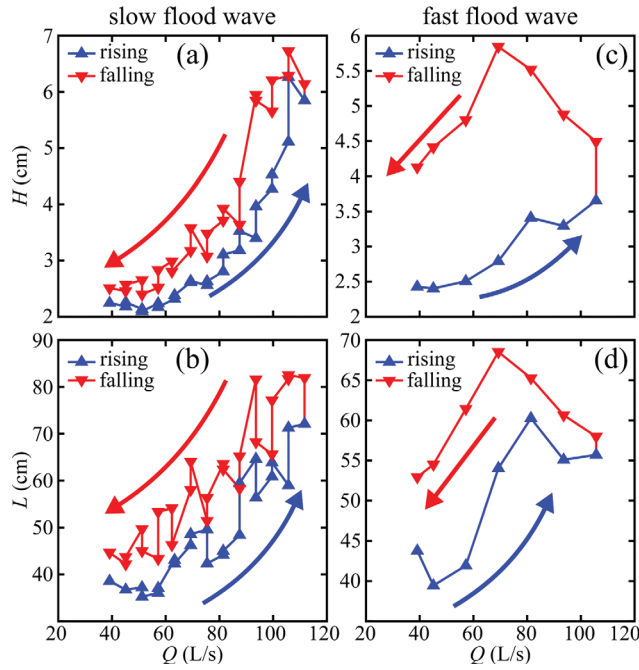
Figure 6. Evolution of bed form heights, H (a and c), and lengths, L (b and d), versus discharge, Q, for the slow (a and b) and fast (c and d) flood waves. Values for rising adjustment are shown in blue with upward facing triangles; values for falling adjustment are shown in red with downward facing triangles. For the slow flood wave, the relationships among H, L, and Q are roughly equivalent for both limbs of the flood wave, with only a small degree of hysteresis apparent. In contrast, H and L hysteresis is substantial in the fast flood wave. Bed forms continue to grow past the flood peak and only start to decrease in size halfway through the flood falling limb.

mean equilibrium Q_2 relict bed form (Figure 7b). This gives

$$V_1 = \beta\phi H_1 L_1 \left(\frac{L_2}{L_1}\right) = \beta\phi H_1 L_2, \tag{5}$$

$$V_2 = \beta\phi H_2 L_2. \tag{6}$$

As shown in Figure 7, H_1 and L_1 (H_2 and L_2) are the Q_1 (Q_2) mean equilibrium bed form heights and lengths, respectively. V_1 and V_2 are outlined by the dashed boxes in Figure 7.

[36] Translation sediment fluxes are determined from the products of equilibrium heights and celerities, as in equation (2):

$$q_{s,1}^t = \beta\phi c_1 H_1, \tag{7}$$

$$q_{s,2}^t = \beta\phi c_2 H_2. \tag{8}$$

[37] Earlier, we observed that $\beta \approx 0.5$ throughout the experiments. Assuming that $\beta = 0.5$ (which also corresponds to the shape factor for idealized triangular bed forms), and substituting into equations (9) and (10), we get:
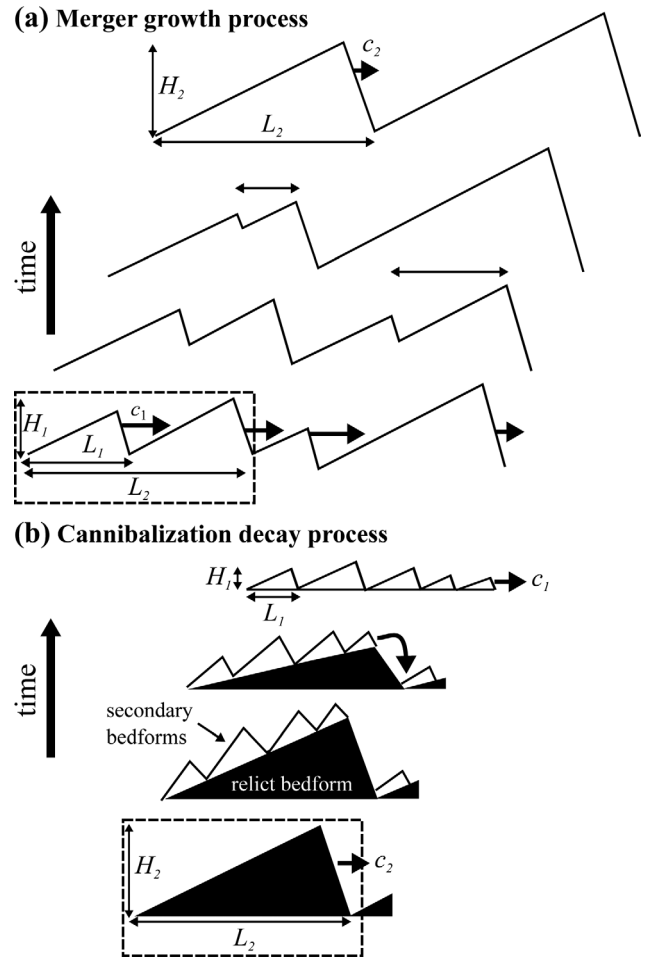

Figure 7. Conceptualization of bed form growth and decay processes. (a) For the growth process, differences among celerities cause bed forms to collide and merge into larger features until a new equilibrium is reached. (b) For the decay process, secondary bed forms (white) migrating across the larger relict flood peak bed form (black) erode the relict crest and fill the relict trough. H_1, L_1, and c_1 refer to low flow mean equilibrium bed form quantities, while H_2, L_2, and c_2 are for high flow. For illustrative purposes, H_1, L_1, etc., are drawn next to individual bed forms, but these in fact refer to mean equilibrium quantities. Dashed boxes outline reconstitution volumes V_1 for merger growth and V_2 for cannibalization decay.

$$T_{12}^r = \frac{H_1 L_2}{H_2 c_2}, \tag{9}$$

$$T_{21}^r = \frac{H_2 L_2}{H_1 c_1}. \tag{10}$$

5.2. Bed-Form Adjustment Normalizations

[38] We define t_{12}^* and t_{21}^* as times from the rising and falling discharge transitions normalized by bed form reconstitution times:

$$t_{12}^* = \frac{t_{12}}{T_{12}^r} = \frac{t_{12} H_2 c_2}{H_1 L_2}, \tag{11}$$

$$t_{21}^* = \frac{t_{21}}{T_{21}^r} = \frac{t_{21} H_1 c_1}{H_2 L_2}. \tag{12}$$

As in section 4, t_{12} is the time from the rising discharge change ($Q_1 \rightarrow Q_2$), and t_{21} is the time from the falling discharge change ($Q_2 \rightarrow Q_1$).

[39] We normalize timeseries of bed form dimensions so that heights and lengths are 1 and 2 at initial and final equilibria, respectively. These normalizations are

$$H^* = \frac{H + H_2 - 2H_1}{H_2 - H_1}, \tag{13}$$

$$L^* = \frac{L + L_2 - 2L_1}{L_2 - L_1}. \tag{14}$$

[40] As noted in section 3, errors in experimental implementation meant that calculated equilibrium bed form and hydraulic quantities differed for nominally equal discharges. To make the appropriate calculations when computing adjustment time scales for individual experiments, we henceforth base these calculations for individual experiments on the relevant experimental segments listed in Table 1, i.e., $H_1 = H_{1a}$, $L_1 = L_{1a}$, and $c_1 = c_{1a}$ for rising adjustments while $H_1 = H_{1b}$, $L_1 = L_{1b}$, and $c_1 = c_{1b}$ for falling adjustments.

5.3. Rising Adjustment Comparison

[41] Normalized rising bed form adjustment curves are plotted together in Figure 8. While there is considerable scatter in the form of the adjustment process, all adjustments took about $10t_{12}^*$ to progress from initial (H^* and $L^* = 1$) to final (H^* and $L^* = 2$) equilibria. Furthermore, heights (Figure 8a) and lengths (Figure 8b) both appear to have followed the same adjustment process. This is despite the fact that equilibrium bed form dimensions and celerities differed considerably among experiments. While growth is slower than decay relative to reconstitution time, growth often progresses more quickly in absolute time due to the much larger sediment fluxes driving bed form growth.

5.4 Falling adjustment comparison

[42] Normalized falling bed form adjustment curves are plotted together in Figure 9. Despite some scatter (particularly in experiments S2 and D1), the overall pattern is the same: rapid decline from initial large dimensions (H^* and $L^* = 2$), followed by asymptotic convergence to equilibrium low values (H^* and $L^* = 1$). Unlike the rising adjustment, however, here the normalized time scale of adjustment is faster, with equilibrium achieved when $t_{21}^* \approx 1$. In other words, the falling bed form adjustment time corresponds roughly to the bed form reconstitution time, T_{21}^r. The adjustment appears to follow an exponential decay.

6. Models for Bed-Form Growth and Decay

[43] The qualitative observations described in section 4.1 indicate the important role of bed form merger in causing bed forms to grow following an increase in discharge, while observations described in section 4.2 indicate that bed form decay progresses through the action of secondary bed forms eroding relict bed form crests and filling relict
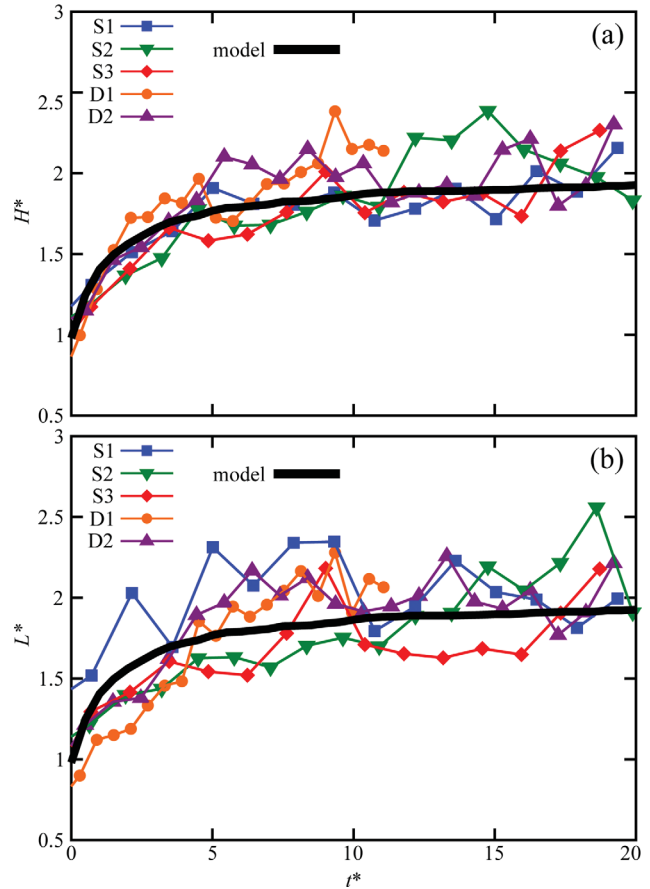

Figure 8. Bed form size adjustments following a step increase in water discharge. (a) Evolution of normalized bed form heights, H^*, and (b) lengths, L^*, compared to the bed form growth model (Figure 12). Based on the assumption of constant bed form steepness, H^* and L^* predictions are equivalent. While the observations indicate a large degree of variability, especially for L^*, the adjustment in general took about $t_{12}^* \approx 10$ or $T_{12}^a = 10T_{12}^r$. These observations are supported by the model curves.

bed form troughs. Here, we present phenomenological models that account for the distinctive processes of bed form growth and decay. The bed form growth model considers how a dispersion of initial bed form sizes, with celerities inversely proportional to lengths, and combine according to simple rules of merger and pass-through. The bed form decay model is built on a diffusion equation with diffusivity based on translation sediment flux.

6.1. Bed-Form Growth Model

[44] Bed forms move with varying celerities, causing them to collide. Merger interactions produce bed form growth while pass-through interactions maintain the size of bed forms. To better understand how these interactions contribute to bed form growth, we built a simple one-dimensional numerical model to phenomenologically reproduce the dynamics of merging bed forms. Our model is adapted from the models of *Fuhrboter* [1983] and
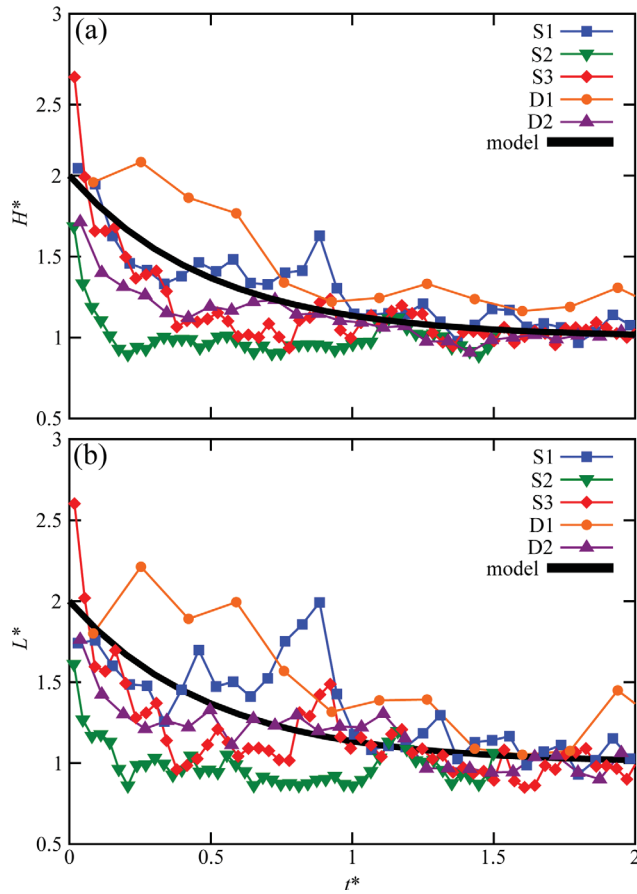
Figure 9. Bed form size adjustments following a step decrease in water discharge. (a) Evolution of normalized bed form heights, H^*, and (b) lengths, L^*, compared to the bed form decay model (equations (26) and (27)). As with bed form growth, the observations indicate a large degree of variability. Nonetheless, the H^* and L^* adjustments took about $t_{21}^* \approx 1$ or $T_{21}^a = T_{21}^r$.

Raudkivi and Witte [1990], though our model offers significant refinements to their treatments.

[45] Based on equation (2), we can directly relate celerities, c_i, and lengths, L_i, of individual bed forms:

$$c_i = \frac{q_s^t}{\phi \beta (H/L) L_i}. \tag{15}$$

Based on observations, we assume constant values of q_s^t, ϕ, β, and H/L through the bed form adjustment. Equation (15) thus shows how c_i are inversely proportional to L_i for individual bed forms.

[46] Based on crestline mapping as shown in Figure 1f, we determined distributions of L_i for each equilibrium segment of the experiments. These are shown in Figure 10. Individual bed form lengths, determined from crest-crest distances, are plotted normalized with respect to mean lengths, L, for each run segment, taken from Table 1 (L_{1a}, L_2, and L_{2a}). Two patterns are apparent in the distributions of bed form lengths. First, the lengths are unimodal, with a clear rightward skew in the distributions. A variety of distributions could be fit to these curves [*van der Mark et al.*,

2008]; the simplest choice is a gamma distribution. While not a perfect fit (e.g., missing the sharp peaks), the gamma offers a decent fit with a minimum of parameters. Second, the modes for the normalized L_i distributions shift rightward and become less skewed (i.e., the gamma shape parameters increase) at higher discharges. For each equilibrium segment, we determined a gamma shape parameter, k^L, for bed form lengths based on maximum likelihood estimation. These shape parameters for individual experimental segments are listed in Table 1. (Because the distributions were normalized by their mean values, calculation of gamma scale parameters was unnecessary.)

[47] We performed five model simulations, with initial conditions chosen to correspond with the Q_{1a} equilibrium parameters described in Table 1. Initial lengths of individual bed forms were chosen at random from a gamma distribution with shape parameter, k_{1a}^L, and mean length, L_{1a}. Initial celerities were then determined based on equation (15), with H_{1a}/L_{1a} from Table 1 and constant $\varphi = 0.58$ and $\beta = 0.5$. The one-dimensional model domain extended over a length of $x = 100$ m, long enough to ensure statistical convergence of model results. The initial bed form lengths were used to determine x-locations of individual bed form crestlines along the domain. Periodic boundary conditions were employed such that bed forms leaving the domain at $x = 100$ m reentered at $x = 0$ m.

[48] Individual crestlines moved rightward along the domain with celerities dependent on their lengths. Collision of adjacent crestlines due to their differing celerities caused bed forms to interact, as demonstrated in Figure 11. As a trailing bed form approached an adjacent bed form ahead, the trailing bed form rose up the stoss slope of the leading bed form until the intervening trough between the two crestlines rose above the zero-line of the domain. For the
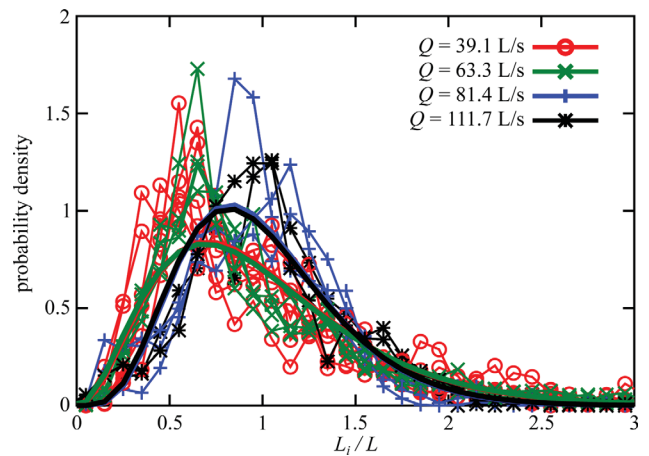

Figure 10. Probability densities of normalized bed form lengths, L_i/L, at steady flow in equilibrium segments of the step discharge adjustment experiments. L for each plotted curve is taken from the appropriate equilibrium segment in Table 1 (L_{1a}, L_2, and L_{1b}). The thick curves show gamma distributions based on the mean gamma shape parameters, k^L, for individual discharge levels. The shape parameters for length distributions tend to increase for higher discharges, indicated as a rightward shift in the distributions. k^L for individual experimental segments are listed in Table 1.
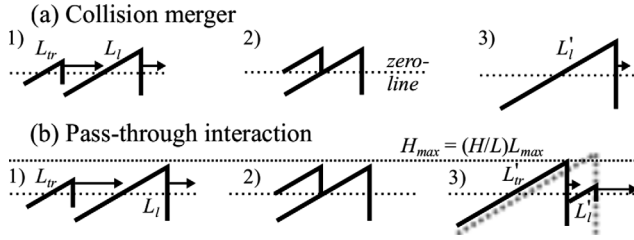
Figure 11. Diagram describing interactions in the bed form merger growth model. Bed forms are treated as right triangles with constant steepness, H/L, which move with celerities inversely proportional to their sizes. (a) For collision merger: (1) a small bed form (with length L_{tr}) approaches a larger one (with length L_l) from behind. (2) When the small bed form is sufficiently close, the intervening trough rises above the dashed zero-line, and they are considered merged. (3) Heights and lengths of colliding bed forms are combined additively to form the new merged bed form (with length L_l'). (b) For pass-through interaction: (1) a small bed form approaches and (2) merges as before. (3) However, the resulting merged form would exceed $H_{\max}$ (and thus also $L_{\max}$ for assumed constant H/L). Instead, a merged form at the maximum height line is formed (with length L_{tr}'), and excess sediment is ejected as a small bed form off the front of the new merged bed form (with length L_l').

zero-crossing method described earlier for delineating individual bed forms, rise of the trough above the zero-line makes the two adjacent bed forms appear effectively as one. Based on this fact, we assumed that a bed form interaction occurred when the distance between two adjacent crestlines dropped to half the length of the leading bed form. This condition also corresponds roughly to interaction of the upstream bed form flow separation bubble with the downstream bed form.

[49] Two outcomes were possible for interacting bed forms in our model: merger and pass-through. The merger interaction, shown in Figure 11a, caused the trailing and leading bed forms to combine additively. The pass-through interaction, shown in Figure 11b, caused exchange of mass from the leading to the trailing bed form.

[50] We defined the merger interaction quantitatively as follows:

$$\text{If } L_{\mathrm{tr}} + L_l \leq L_{\max}, \text{ then } \begin{cases} L_{\mathrm{tr}}' \rightarrow \text{eliminated}. \\ L_l' = L_{\mathrm{tr}} + L_l. \end{cases} \quad (16)$$

L_{tr} and L_l refer to the lengths of trailing and leading bed forms, respectively, prior to interaction, and the primed quantities (L_{tr}' and L_l') refer to post-interaction lengths. $L_{\max}$ is the maximum bed form size (to be described below). When the sum of L_{tr} and L_l is less than $L_{\max}$, the bed forms merge. As indicated by the equation, the trailing bed form is eliminated while the new leading bed form length sums the original bed form lengths. The additive nature of bed form merger lengthening in our model is necessitated by the assumption of constant H/L.

[51] We defined the pass-through interaction quantitatively as follows:

$$\text{If } L_{\mathrm{tr}} + L_l > L_{\max}, \text{ then } \begin{cases} L_{\mathrm{tr}}' = \min\left(L_{\max}, L_{\mathrm{tr}} + L_l - L_{\min}\right), \\ L_l' = \max\left(L_{\max} - L_l, L_{\min}\right). \end{cases} \quad (17)$$

Here, $L_{\min}$ refers to the minimum allowable bed form length, taken as $L_{\min} = 8.3$ mm as in section 3. Most pass-through interactions transfer leading bed form mass to the trailing bed form so that $L_{\mathrm{tr}}' = L_{\max}$, while the remaining bed form mass makes up the new L_l'. However, our model enforces a minimum condition such that $L_l' \geq L_{\min}$; otherwise, the pass-through would produce unrealistically small bed forms.

[52] The $L_{\max}$ condition separating bed form merger and pass-through restricts the runaway growth of bed forms. It is thought that the water free surface limits vertical bed form growth [e.g., *Gill*, 1971; *Coleman and Fenton*, 2000; *Fourriere et al.*, 2010], though aeolian dunes, where such free-surface limitations are lacking, also display pass-through interactions possibly related to the orientations and relative sizes of colliding bed forms [*Duran et al.*, 2005; *Diniega et al.*, 2010]. For simplicity, we assumed the maximum bed form height, $H_{\max}$, to be the equilibrium height of bed forms at Q_2, i.e., $H_{\max} = H_2$. Because we also assumed constant steepness, we thus assumed that $L_{\max} = \frac{H_{\max}}{H/L}$. (While we have taken bed form height as the limiting quantity here, our model considers bed form lengths because of their direct connection to crestline interactions.)

[53] Following each merger and pass-through interaction in our model, bed form celerities were recalculated according to equation (15). By a series of interactions, bed form lengths grew asymptotically toward $L_{\max}$, and heights grew proportionally with lengths according to the assumed constant H/L. An example of a merger model simulation, based on the parameters of the S2 experiment, is shown in Figure 12. The crestline plots in Figures 12a and 12b show how the model qualitatively reproduces the experimentally observed lengthening and reduction in number of bed forms through time. It also shows how the model reproduces (and somewhat exaggerates) pass-through interactions, indicated by waves of high celerity that occasionally pass among multiple bed forms.

[54] The modeled increase of mean bed form height, L, is shown in Figure 12c in comparison to S2 experimental observations. For both model and experiment, time to equilibrium is about 5000 s, though the model shows an initially faster rise in L while the observations show a greater degree of L variability on the path to equilibrium. In Figure 12d, the model runs based on parameters for all five step-adjustment experiments are compared in normalized units of L^* and t^*. The results of all the simulations are very similar. We thus choose to represent the general form of the bed form growth process by a mean L^* versus t^* curve averaging over all the simulations.

[55] The modeled mean bed form height and length-growth curves are compared to observations for all step adjustment experiments in Figure 8. Note that the modeled H^* is simply the modeled L^* multiplied by the assumed constant H/L for all the experiments. The model accurately
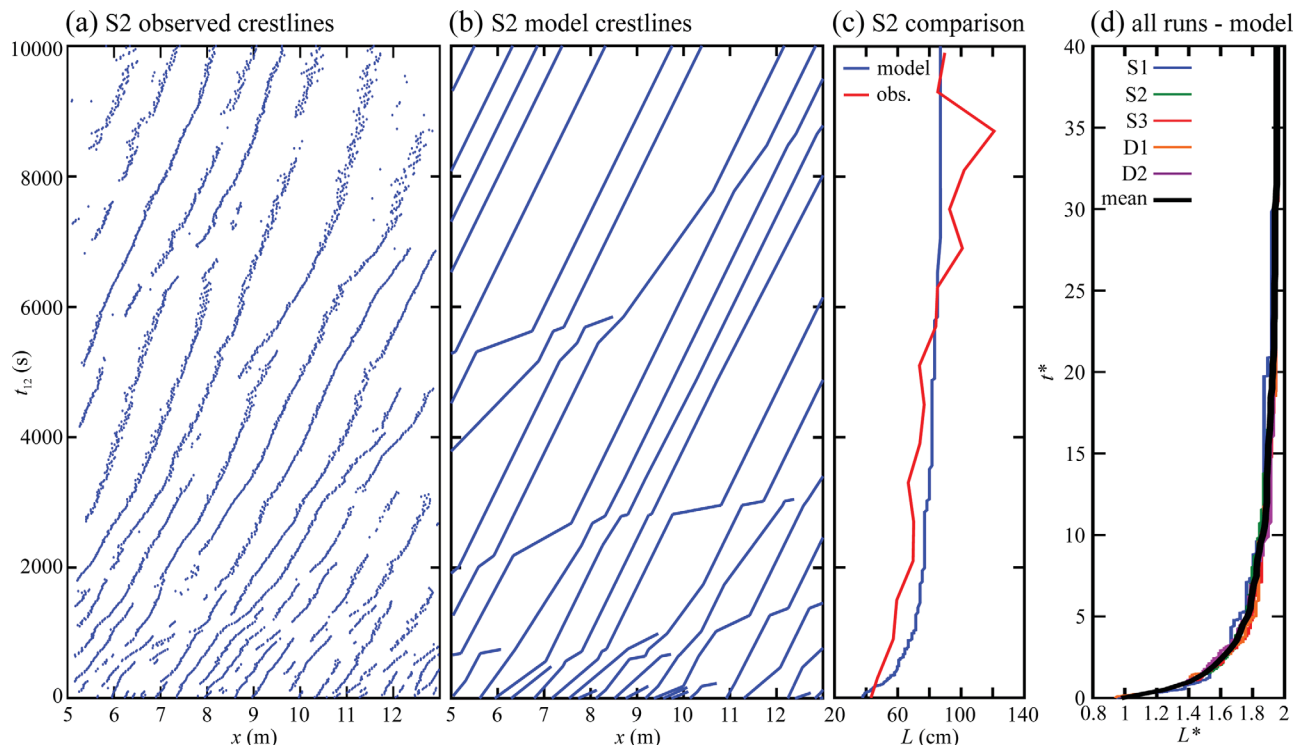
Figure 12. (a) Example of crestline evolution during rising adjustment in experiment S2, with time, t_{12}, from the step discharge transition. (b) The merger model was parameterized with equilibrium values from experiment S2, resulting in the crestline evolution shown here. To obtain better statistics, the full model was run over a length of 100 m, but only an 8 m section is shown here for comparison to observations. As in the observed case, the density of crestlines declines rapidly from the discharge change, and celerities correspondingly decrease. However, small segments of high celerity indicate ejection of small bed forms during pass-through interactions. Such interactions are particularly common for $t_{12} = 1000$–2000 s in both observations and model, though the model tends to exaggerate these interactions somewhat. (c) The model prediction of growth in bed form length, L, corresponds well with observations. Differences appear to arise due to variability in the observed curve. (d) The merger model was run based on parameters from all of the adjustment experiments. The model curves are all very similar in normalized time, t^*, and length, L^*, coordinates. The thick black mean curve is used for comparison to observations in Figure 8.

reproduces the general growth patterns of H^* and L^*. Discrepancies between model and observations appear to occur due to scatter in the observed height and length growth curves. As observed, the normalized time for adjustment is $t_{12}^* \approx 10$. Defining T_{12}^a as the time scale for bed form growth adjustment, we thus have that $T_{12}^a = 10T_{12}^r$.

6.2. Bed-Form Decay Model

[56] Observations described in section 4.2 indicate that bed form decay progresses through the action of secondary bed forms eroding relict bed form crests and filling relict bed form troughs. The nature of the decay process indicates that it acts like diffusion, i.e., the rate of decay is proportional to the elevation gradient between relict bed form crests and troughs. Here, we adopt a simple diffusion model to quantitatively describe the bed form decay process.

[57] Adapting the definitions of reconstitution volumes described in equations (5) and (6), we define equilibrium

crest (top) volumes, V_1^{top} and V_2^{top}, for bed forms at low and high flows, respectively:

$$V_1^{\text{top}} = (1/2)V_1 = (1/2)\beta\phi H_1 L_2, \tag{18}$$

$$V_2^{\text{top}} = (1/2)V_2 = (1/2)\beta\phi H_2 L_2. \tag{19}$$

The 1/2 terms reflect the fact that we are considering only the top half of bed form volumes. (A similar derivation based on the bottom half of bed forms would arrive at an equivalent result by symmetry.) We also define

$$V^{\text{top}} = (1/2)\beta\phi H L_2. \tag{20}$$

V^{top} and H are variables describing how the top half sediment volume and mean bed form height, respectively, develop through time, t_{21}, from the step discharge drop.

[58] Assuming that the rate of change of V^{top} depends on translation sediment flux, q_s^t, and the difference in top

sediment volume relative to equilibrium, we define a diffusion equation:

$$\frac{\mathrm{d}V^{\mathrm{top}}}{\mathrm{d}t_{21}} = -\left(\frac{V^{\mathrm{top}} - V_1^{\mathrm{top}}}{V_2^{\mathrm{top}}}\right)q_s^t. \tag{21}$$

The initial condition is

$$V^{\mathrm{top}}(t_{21} = 0) = V_2^{\mathrm{top}}. \tag{22}$$

Combining equations (21) and (22), we get

$$V^{\mathrm{top}} = \left(V_2^{\mathrm{top}} - V_1^{\mathrm{top}}\right)\exp\left(-\frac{q_s^t}{V_2^{\mathrm{top}}}t_{21}\right) + V_1^{\mathrm{top}}. \tag{23}$$

Substituting the top volumes from (18), (19), and (20) into (23), we get an equation for bed form height evolution:

$$H = (H_2 - H_1)\exp\left(-\frac{2q_s^t}{\beta\phi H_2 L_2}t_{21}\right) + H_1. \tag{24}$$

Based on the definition of q_s^t in (2), (24) becomes

$$H = (H_2 - H_1)\exp\left(-\frac{2H_1 c_1}{H_2 L_2}t_{21}\right) + H_1. \tag{25}$$

Finally, normalization by (12) and (13) gives

$$H^* = \exp\left(-2t_{21}^*\right) + 1. \tag{26}$$

Based on the assumption of constant H/L, we adopt an identical model equation for normalized bed form length adjustment:

$$L^* = \exp\left(-2t_{21}^*\right) + 1. \tag{27}$$

[59] Equations (26) and (27) for the bed form decay model are compared to observations in Figure 9. The plots indicate general agreement between our decay model and observations, with a falling adjustment time scale of $T_{21}^a = T_{21}^r$ corresponding to $t_{21}^* = 1$. However, the observed bed form decay adjustments, especially those for bed form lengths, provide only limited evidence for the exponential form of the decay model. In the case of bed form lengths, the definition of bed form lengths based on the zero-crossing method may contribute to the observed variability due to the presence of distinctive relict and secondary bed form length scales.

7. Origin of Bed-Form Hysteresis

7.1. Conceptual Model

[60] Our experiments and models indicate that bed forms adjust to abrupt changes in flow at time scales proportional to reconstitution times, which are related to equilibrium bed form heights, lengths, and celerities. When discharge changes are not abrupt but progress gradually over the course of a flood wave, the occurrence of lagged bed form adjustment and hysteresis appears to be related to the time scale of discharge change.

[61] Based on these experimental results, we hypothesize that bed form hysteresis occurs when the time scales of flood wave discharge change are shorter than time scales of bed form adjustment. In other words, hysteresis arises due to lagged response in bed form size relative to discharge. This can occur on the flood rising limb, falling limb, or both. Quantitatively, we predict that bed form lags (and thus hysteresis) occur when:

$$T_{12}^Q < T_{12}^a = 10T_{12}^r = \frac{10H_1 L_2}{c_2 H_2} \quad, \quad \text{and/or} \tag{28}$$

$$T_{21}^Q < T_{21}^a = T_{21}^r = \frac{H_2 L_2}{c_1 H_1}. \tag{29}$$

Here, T_{12}^Q and T_{21}^Q refer to the durations of flood wave discharge increase and decrease, respectively, determined from the hydrograph. Equations (28) and (29) predict when bed form lags occur in response to rising and falling discharge changes, respectively.

7.2. Application to Flood Wave Experiments

[62] To test this hypothesis, we calculate T_{12}^a and T_{21}^a for the flood wave experiments based on the equilibrium bed form heights, lengths, and celerities from step discharge experiment S1, for which the minimum and maximum discharges were the same as for the flood wave experiments. Based on Table 1, these are

$$T_{12}^a \approx 10T_{12}^r = 10\frac{H_1 L_2}{H_2 c_2} = 4140\,\mathrm{s} \approx 1.2\,\mathrm{h}. \tag{30}$$

$$T_{21}^a \approx T_{21}^r = \frac{H_2 L_2}{H_1 c_1} = 19{,}300\,\mathrm{s} \approx 5.4\,\mathrm{h}. \tag{31}$$

We note here that, in absolute terms, T_{21}^a is significantly larger than T_{12}^a, despite the fact that T_{12}^a is larger in relative terms. This is because T_{21}^r incorporates both larger bed forms and smaller celerities than T_{12}^r.

[63] For the slow flood, $T_{12}^Q = T_{21}^Q = 4\,\mathrm{h}$, much longer than T_{12}^a and slightly shorter than T_{21}^a. Based on these results, equations (28) and (29) predict a small amount of hysteresis due to slight bed form lag on the flood falling limb, as we indeed observe in Figures 5a–5c and 6a and 6b. In contrast, for the fast flood, $T_{12}^Q = T_{21}^Q = 1\,\mathrm{h}$, slightly shorter than T_{12}^a and significantly shorter than T_{21}^a, predicting a large amount of hysteresis due to lags on both flood limbs, though primarily in the falling limb. Again, this prediction agrees with observations (Figures 5d–5f and 6c and 6d). In particular, H and L decay for about 4 h past the flood peak, in agreement with the calculated T_{21}^a time scale.

7.3. Application to Natural Rivers

[64] Bed form adjustments in natural river flood waves further illustrate the utility of our hypothesized adjustment time scales. We compare three flood waves with varying degrees of hysteresis. The first, with only slight hysteresis noted, was observed by *Gabel* [1993] on the medium-sized Calamus River in Nebraska (Q range: 1.02–1.79 m³/s) and spanned 2 weeks. The second, with substantial hysteresis, was observed by *Wilbers and Ten Brinke* [2003] on the

Table 2. Parameters for Natural Flood Waves Examined in Section 7.3[a]

Location	T_{12}^{Q}	T_{21}^{Q}	H_1	L_1	c_1	H_2	L_2	c_2	T_{12}^{a}	T_{21}^{a}
Calamus R[b]	168 h	168 h	0.097 m	2.02 m	0.98 m/h	0.188 m	3.24 m	1.31 m/h	13 h	6.4 h
Rhine R[c]	168 h	168 h	0.1 m	4 m	0.21 m/h	1.4 m	50 m	2.1 m/h	17 h	3300 h
Clear Run[d]	17.5 min	22 min	1 cm	12 cm	0.9 cm/min	3 cm	75 cm	11.3 cm/min	22.1 min	250 min

[a]T_{12}^{Q} and T_{21}^{Q} refer to durations of rising and falling sections of flood hydrographs, respectively. H_1, L_1, and c_1 are mean equilibrium low-flow bed form heights, lengths, and celerities, respectively, while H_2, L_2, and c_2 are mean equilibrium values for high flows, respectively. T_{12}^{a} and T_{21}^{a} are adjustment time scales for bed form growth and decay, respectively, estimated from equilibrium parameters.
[b]Values are from *Gabel* [1993]. T_{12}^{Q} and T_{21}^{Q} assume 7 day rising and falling limbs, as approximated from hydrograph (Figure 7b in the article). H_1, L_1, and c_1 values are taken for "right-hand channel" on 20 April 1985 in Table 2, while H_2, L_2, and c_2 values are taken for 1 May 1985.
[c]Values are from *Wilbers and Ten Brinke* [2003]. T_{12}^{Q} and T_{21}^{Q} assume 7 day rising and falling limbs, as approximated from hydrograph (Figure 6a in the article). H_1 and H_2, L_1 and L_2, and c_1 and c_2 are estimated from minimum and maximum observations for "1995" in Figures 11a, 10a, and 12a, respectively.
[d]Values are from *Harvey et al.* [2012]. T_{12}^{Q} and T_{21}^{Q} are from section 4.4.1. H_1, L_1, c_1, H_2, L_2, and c_2 are from Table 2.

large Rhine River in Netherlands (Q range: 2500–11,900 m³/s) and also spanned 2 weeks. The third, also with substantial hysteresis, was observed by *Harvey et al.* [2012] on the small Clear Run in North Carolina, for an artificially generated (dam-release) flood wave spanning ≈ 40 min (Q range: 0.06–0.39 m³/s). Bed form parameters for these three flood waves and calculations of T_{12}^{a} and T_{21}^{a} are provided in Table 2.

[65] As indicated in Table 2, $T_{12}^{a} \ll T_{12}^{Q}$ for the Calamus and the Rhine, while T_{12}^{a} was comparable to T_{12}^{Q} in Clear Run. Thus, we expect no (or only a small) contribution of rising limb discharge change to bed form lags. However, while $T_{21}^{a} \ll T_{21}^{Q}$ for the Calamus, $T_{21}^{a} \gg T_{21}^{Q}$ for the Rhine and Clear Run. As predicted by our hypothesis, bed forms experienced substantial hysteresis in the Rhine and Clear Run floods, while the hysteresis in the Calamus flood was slight. In the Calamus, the flood had a long time to displace small bed forms, so bed forms were able to keep pace with flow changes. However, much larger bed forms in the Rhine and much shorter flood duration in Clear Run caused bed form lags and hysteresis to occur. The visual nature of this hysteresis in Clear Run can be seen in *Harvey et al.* [2012, Figure 4].

[66] We admit that our method of estimating equilibrium bed form dimensions from flood data, especially peak values when flows are highly unsteady, is imperfect. Ideally, prediction of hysteresis would depend on independently verified estimates of bed form dimensions made prior to the actual flood wave. Nonetheless, the crudely estimated values for equilibrium bed form parameters appear to provide sufficient information to correctly determine the presence or absence of hysteresis.

8. Discussion

8.1. Interpretation of Models

[67] Our observations of bed form lags and hysteresis reproduce similar effects as those observed by *Gee* [1975], *Wijbenga and Klaassen* [1983], and *Wijbenga and Van Nes* [1986]. Specifically, the observations of *Gee* [1975] and *Wijbenga and Klaassen* [1983] agree with our finding that, relative to bed form reconstitution time, T_{12}^{a} is larger than T_{21}^{a}. Our observation that shorter flood waves produce a greater magnitude of hysteresis agrees with *Wijbenga and Van Nes* [1986]. However, unlike the previous bed form adjustment models of *Allen* [1976b, 1976c, 1976d] and *Fredsoe* [1979], which failed to explain experimental and field observations, our models for bed form adjustment

accurately predict time scales of bed form adjustment and occurrence of bed form hysteresis. Also, as far as we know, ours is the first model to predict the process and time scale of bed form decay.

[68] Our hypothesis for predicting the occurrence of bed form hysteresis, confirmed by experimental and field data, offers a straightforward method that depends only on the estimation of a few geometric parameters. This method is built on observations about the way in which bed forms interact through merger, pass-through, and cannibalization. Given the limited longitudinal view of flume bed form evolution in our experiments, the modeled bed form interactions simplify a more complex set of bed form interactions (e.g., defect migration, repulsion, calving, lateral linking, and solitary wave behavior) observable in planform view [e.g., *Schwammle and Herrmann*, 2003; *Endo et al.*, 2004; *Kocurek et al.*, 2010; *Vermeesch*, 2011]. Nonetheless, because our models capture the essential mass balance of bed form interactions, they are able to accurately predict adjustment time scales.

[69] Our models do not depend on understanding the hydrodynamic processes underlying the formation, migration, or equilibrium dimensions of bed forms. Therefore, possible morphological distinctions between ripples and dunes should not influence estimates of adjustment time scales. However, typical bed form stability diagrams [e.g., *Southard*, 1991] do predict that our experimental bed forms should have experienced a transition from ripples (which scale with grain size [e.g., *Baas*, 1994]) to dunes (which scale with flow depth [e.g., *van Rijn*, 1984]). It is argued that the ripple-dune transition arises from a change in the nature of flow turbulence related to particle Reynolds number [e.g., *Yalin*, 1964] and that this could affect the transient ripple-dune transition [*Robert and Uhlman*, 2001]. Equations describing the dependence of ripple and dune dimensions on hydraulic and grain parameters could potentially be used for prediction of bed form adjustment time scales in our models. However, observations typically display a wide range of variability relative to these equations [e.g., *Julien and Klaassen*, 1995], while our prediction of adjustment time scales based on directly observed equilibrium bed form dimensions is not subject to the uncertainty of these equations.

[70] An important assumption of our models is that of constant bed form steepness (H/L). However, the bed form adjustments to flood waves described above show varying degrees of steepness change. The relatively greater increase of bed form heights versus lengths shown in Figure 5 indicates slight steepening of bed forms around the flood peak

in our experimental flood waves, and this is also observed in the Calamus flood [*Gabel*, 1993]. However, bed forms in the Rhine [*Wilbers and Ten Brinke*, 2003] and Clear Run [*Harvey et al.*, 2012] show an opposite decrease in steepness at the flood peak. On the flood falling limb, in fact, Rhine bed form lengths continue to grow indefinitely while bed form heights shrink [*Wilbers and Ten Brinke*, 2003]. These different steepness responses may simply reflect the complications in measuring bed form lengths on the falling limb when secondary bed forms coexist with relict bed forms. Changes in steepness may also reflect the fundamental differences between bed form growth and decay processes and different relative rates of bed form length and height changes through these adjustments [*Wijbenga and Van Nes*, 1986; *Wilbers and Ten Brinke*, 2003; *Nelson et al.*, 2011]. While our bed form growth model suggests that growth primarily depends on bed form lengthening through crestline interactions, our bed form decay model depends on the shrinking height of relict bed forms through diffusion. Differing degrees of overlap in the length-based growth and height-based decay processes could then explain differences in steepness evolution.

8.2. Limitations of Bed-Form Adjustment Time Scale Estimates

[71] We now note a few potential issues with our adjustment time scales in addition to those already mentioned. First, our models are built on limited experimental data, for which bed forms display broad variations in dimensions and celerities that do not completely converge to mean values for the limited length of our flume. Second, our models assume no hysteresis in the relationship between q_s^t and Q, while in fact q_s^t should vary as flow resistance changes with changing bed form dimensions [e.g., *van Rijn*, 1984, *Wilbers and Ten Brinke*, 2003, *Paarlberg et al.*, 2010]. Our observations indicate abrupt adjustment of q_s^t to Q on the rising limb (e.g., Figure 2i); however, due to problems in calculating q_s^t on the falling limb, described in section 4.2, we could not evaluate this error for our bed form decay model predictions. Third, our models assume that bed form reconstitution is entirely driven by translation sediment flux, while neglecting suspended load and other nontranslation components that may also contribute significantly to bed form change, especially in natural rivers with lower Rouse numbers (*P*) [*McElroy and Mohrig*, 2009]. We note that while suspended sediment flux was likely substantial for higher discharge segments of our experiments (i.e., $Q = 81.1$ and 111.7 L/s), as indicated by *P* values near unity (Table 1) and total sediment fluxes, q_s (section 2), much larger than q_s^t (Table 1), our time scale predictions utilizing only q_s^t provided good predictions. However, we suspect experimental error in our measurements of total q_s, because calculated equilibrium q_s^t at low discharges (i.e., $Q = 39.1$ and 63.3 L/s) are inexplicably lower than measured total q_s for the same discharges.

[72] Application of abrupt discharge change bed form adjustment time scales to flood waves with gradually increasing and decreasing discharge raises some additional issues. First, the high-flow q_s^t used for prediction of T_{12}^a in equation (28) should be larger than the true q_s^t, which increases gradually to the peak value over the flood rising limb, thus equation (28) is probably an underprediction of T_{12}^a. Conversely, equation (29) is probably an overprediction of T_{21}^a. Second, spatial heterogeneity in bed morphology and granularity complicate predictions of bed form adjustment [e.g., *Frings and Kleinhans*, 2008]. Third, the flume tailgate in our experiments imposed a backwater curve that caused flows to adjust primarily through changes in water surface slope rather than flow depth, in contrast to natural floods [e.g., *Julien et al.*, 2002] and previous experiments [*Gee*, 1975; *Wijbenga and Klaassen*, 1983; *Wijbenga and Van Nes*, 1986]. Backwater effects may have introduced spatial nonuniformity in sediment fluxes and bed form sizes, though our experimental data indicated no significant spatial trends. However, we argue that, because our bed form adjustment models depend only on celerities and geometric properties of bed forms in equilibrium, the specific hydraulic processes driving bed form change (either by depth or velocity changes) are irrelevant to prediction of bed form adjustment times.

8.3. Implications of Bed-Form Adjustment Lags

[73] Some of the observed uncertainty and variability in natural bed form geometries, described in section 1, may be related to the delayed response of bed forms to unsteady flows, particularly in large rivers. As shown in Table 2, our model predicts a 3300 h (140 day) adjustment time for bed form decay following the large flood on the Rhine. In fact, it is possible in very large rivers, particularly those with large annual ranges of discharge variation, which bed forms may never be fully in equilibrium with discharge. Indeed, many authors have argued that polymodal dune assemblages in rivers arise due to multiple bed form sizes forming under multiple different flows [*Jones*, 1977; *Allen*, 1978; *Rubin and McCulloch*, 1980]. The importance of lagged bed form adjustment is already well recognized in aeolian systems, where dune geometries may remain stable through thousands of years under altered wind conditions, simply because the reconstitution time scale is small compared to the size of relict features [*Lancaster*, 1988; *Warren and Allison*, 1998; *Bristow et al.*, 2007]. Aeolian dune fields may simultaneously contain three or four size classes of bed forms, from ripples responding to minute-scale winds to megadunes responding to wind regimes defined over thousands of years [*Lancaster*, 1988; *Warren and Allison*, 1998; *Kocurek and Ewing*, 2005; *Ewing and Kocurek*, 2010]. Informed by theoretical equilibrium bed form sizes and records of water discharge or wind speed at sites of interest, our estimates of bed form adjustment time scales could provide scientists and practitioners with a simple method to estimate whether or not observed bed forms are in fact in equilibrium with flow conditions.

[74] Lagged bed form response presents important implications for flow hydraulics. Bed forms extract fluid momentum by form drag, and the size of bed features can have a dramatic effect on the bed friction factor [*Brooks*, 1958; *Engelund and Hansen*, 1967; *Gee*, 1975; *Engelund and Fredsoe*, 1982; *van Rijn*, 1984; *Wiberg and Nelson*, 1992; *Li*, 1994; *Nelson et al.*, 2011; *Paarlberg et al.*, 2010]. Differences in friction between flood rising and falling limbs can in turn produce nonuniqueness in stage-discharge relationships [*Simons and Richardson*, 1962; *Jordan*, 1965; *Gee*, 1975; *Shimizu et al.*, 2009; *Paarlberg et al.*, 2010]. Large losses by form drag also reduce the

skin friction available for sediment transport, producing accompanying hysteresis in sediment flux [*Ten Brinke et al.*, 1999; *Wilbers and Ten Brinke*, 2003; *Paarlberg et al.*, 2010]. In our experiments, persistence of relict topography appears to have significantly slowed the adjustment of water surface slope following the decrease in water discharge, until bed topography fully transitioned to equilibrium. Our models, by predicting transient evolution of bed-form geometry, could inform predictions of changing flow resistance and hydraulics.

[75] Our bed form adjustment models could also be extended to a variety of other fluvial processes where bed form geometries are important: (1) accumulations of bed form sediments in depositional environments produce potentially useful records of past flow events [e.g., *Paola and Borgman*, 1991; *Leclair*, 2002; *Burr et al.*, 2004; *Grotzinger et al.*, 2005; *Jerolmack and Mohrig*, 2005a; *Leclair and Blom*, 2005; V. Ganti et al., Kinematic controls on the geometrical structure of preserved cross-sets, submitted to *Journal of Geophysical Research*]; however, lagged response of bed form geometries to flow changes means that bed forms record not only flows at the instant of their formation but also a history of recent flows prior to their formation [*Jones*, 1977]. (2) Local variations in fluid pressure over bed forms induce the exchange of solutes and fine particles between surface and pore water with implications for stream ecology [e.g., *Thibodeaux and Boyle*, 1987; *Elliott and Brooks*, 1997a, 1997b], and rates of exchange are strongly linked to discharge, bed form geometries, and bed form celerities [*Packman et al.*, 2000; *Packman and Brooks*, 2001; *Stonedahl et al.*, 2010]. In particular, recent field observations highlight the importance of deep solute flow paths through persistent large relict bed forms during and after the flood-falling limb [*Harvey et al.*, 2012]. (3) Flow nonuniformity, arising from uneven underlying riverbed topography, such as channel bars, produces strong spatial variation in superimposed bed form geometries [*Coleman*, 1969; *Rubin and McCulloch*, 1980; *Flemming*, 2000; *Nittrouer et al.*, 2008]. Bed form adjustments to unsteady flows are directly analogous to these nonuniform dynamics, especially when bed forms adjust their sizes as they migrate. We believe that our bed form growth and decay models could be extended in the future to predict the role of unsteady bed forms in formation of stratigraphy, stream-subsurface exchange, and spatial bed form patterns.

9. Conclusions

[76] We have presented quantitative models, supported by flume observations, which predict the adjustment of fluvial bed forms to abrupt changes in water discharge. Our models are geometric in nature, dependent on a bed form reconstitution time that is based on equilibrium bed form heights, lengths, and celerities before and after discharge changes. The models account for the distinctive processes of bed form growth by merger and decay by secondary bed form cannibalization of relict forms.

[77] Observations of bed form adjustment through experimental flood waves show that hysteresis between bed form geometries and discharge depends on the time scale over which discharge changes. Specifically, we hypothesize that hysteresis occurs when durations of flood rising and falling

limbs are shorter than predicted time scales for bed form adjustment to abrupt flow changes. Calculated bed form adjustment times for our flood wave experiments and for natural flood waves support this argument. While we are not the first to argue that hysteresis arises from lagged bed form response, we have provided the first quantitative metrics for determining when hysteresis should occur.

[78] We anticipate that our models of bed form growth and decay could be extended to modeling bed form response to more complex unsteady flows. Prediction of bed form dimensions in such unsteady flows would prove useful for a variety of applications including prediction of flow resistance, reconstruction of bed form stratigraphy, quantification of bed pressure fields for solute and fine particle exchange in riverbeds, and improved understanding of heterogeneous bed form topography in nonuniform flows.

References

Allen, J. R. L. (1968), The nature and origin of bed form hierarchies, *Sedimentology*, *10*(3), 161–182.

Allen, J. R. L. (1970), *Physical Processes of Sedimentation*, Elsevier, New York.

Allen, J. R. L. (1973), Phase differences between bed configuration and flow in natural environments, *and their geological relevance*, Sedimentology, *20*(2), 323–329, doi:10.1111/j.1365-3091.1973.tb02054.x.

Allen, J. R. L. (1974), Reaction, relaxation and lag in natural sedimentary systems: General principles, examples and lessons, *Earth Sci. Rev.*, *10*(4), 263–342.

Allen, J. R. L. (1976a), Time-lag of dunes in unsteady flows: An analysis of Nasner's data from the R. Weser, Germany, *Sediment. Geol.*, *15*(4), 309–321.

Allen, J. R. L. (1976b), Computational models for dune time-lag: General ideas, difficulties, and early results, *Sediment. Geol.*, *15*(1), 1–53, doi:16/0037-0738(76)90020-8.

Allen, J. R. L. (1976c), Computational models for dune time-lag: Population structures and the effects of discharge pattern and coefficient of change, *Sediment. Geol.*, *16*(2), 99–130.

Allen, J. R. L. (1976d), Bed forms and unsteady processes: Some concepts of classification and response illustrated by common one-way types, *Earth Surf. Processes*, *1*(4), 361–374, doi:10.1002/esp.3290010405.

Allen, J. R. L. (1978), Polymodal dune assemblages: An interpretation in terms of dune creation–destruction in periodic flows, *Sediment. Geol.*, *20*, 17–28.

Allen, J. R. L., and P. F. Friend (1976), Relaxation time of dunes in decelerating aqueous flows, *J. Geol. Soc. London*, *132*(1), 17–26, doi:10.1144/gsjgs.132.1.0017.

Baas, J. H. (1994), A flume study on the development and equilibrium morphology of current ripples in very fine sand, *Sedimentology*, *41*(2), 185–209, doi:10.1111/j.1365-3091.1994.tb01400.x.

Baas, J. H. (1999), An empirical model for the development and equilibrium morphology of current ripples in fine sand, *Sedimentology*, *46*(1), 123–138, doi:10.1046/j.1365-3091.1999.00206.x.

Baas, J. H., and H. DeKoning (1995), Washed-out ripples: their equilibrium dimensions, migration rate, and relation to suspended-sediment concentration in very fine sand, *J. Sediment. Res.*, *65*(2a), 431–435, doi:10.1306/D42680E5-2B26-11D7-8648000102C1865D.

Baas, J. H., A. P. Oost, O. K. Sztano, P. L. Boer, and G. Postma (1993), Time as an independent variable for current ripples developing towards

linguoid equilibrium morphology, *Terra Nova*, *5*(1), 29–35, doi:10.1111/j.1365-3121.1993.tb00223.x.

Bagnold, R. (1941), *The Physics of Blown Sand and Desert Dunes*, Dover, London, U. K.

Bartholoma, A., V. Ernstsen, B. Flemming, and J. Bartholdy (2004), Bed form dynamics and net sediment transport paths over a flood-ebb tidal cycle in the Gradyb channel (Denmark), determined by high-resolution multibeam echosounding, *Danish J. Geog.*, *104*(1), 45–55.

Best, J. (1996), The fluid dynamics of small-scale alluvial bed forms, in *Advances in Fluvial Dynamics and Stratigraphy*, pp. 67–125, Wiley, New York.

Betat, A., V. Frette, and I. Rehberg (1999), Sand ripples induced by water shear flow in an annular channel, *Phys. Rev. Lett.*, *83*(1), 88–91, doi:10.1103/PhysRevLett.83.88.

Bokuniewicz, H., R. Gordon, and K. Kastens (1977), Form and migration of sand waves in a large estuary, Long Island Sound, *Mar. Geol.*, *24*, 185–199, doi:10.1016/0025-3227(77)90027-5.

Bristow, C., G. Duller, and N. Lancaster (2007), Age and dynamics of linear dunes in the Namib Desert, *Geology*, *35*(6), 555–558, doi:10.1130/G23369A.1.

Brooks, N. H. (1958), Mechanics of streams with movable beds of fine sand, *Trans. Am. Soc. Civil Eng.*, *123*, 526–549.

Burr, D. M., P. A. Carling, R. A. Beyer, and N. Lancaster (2004), Flood-formed dunes in Athabasca Valles, Mars: Morphology, modeling, and implications, *Icarus*, *171*(1), 68–83, doi:10.1016/j.icarus.2004.04.013.

Charru, F., B. Andreotti, and P. Claudin (2013), Sand ripples and dunes, *Annu. Rev. Fluid Mech.*, *45*(1), doi:10.1146/annurev-fluid-011212-140806.

Coleman, J. M. (1969), Brahmaputra River: Channel processes and sedimentation, *Sediment. Geol.*, *3*(2-3), 129–239, doi:10.1016/0037-0738(69)90010-4.

Coleman, S., and B. Eling (2000), Sand wavelets in laminar open-channel flows, *J. Hydraul. Res.*, *38*, 331–338, doi:10.1080/00221680009498314.

Coleman, S. E., and J. D. Fenton (2000), Potential-flow instability theory and alluvial stream bed forms, *J. Fluid Mech.*, *418*, 101–117.

Coleman, S. E., and B. W. Melville (1994), Bed form development, *J. Hydraul. Eng.*, *120*(5), 544–560, doi:10.1061/(ASCE)0733-9429(1994)120:5(544).

Coleman, S. E., and B. W. Melville (1996), Initiation of bed forms on a flat sand bed, *J. Hydraul. Eng.*, *122*, 301–310, doi:10.1061/(ASCE)0733-9429(1996)122:6(301).

Diniega, S., K. Glasner, and S. Byrne (2010), Long-time evolution of models of aeolian sand dune fields: Influence of dune formation and collision, *Geomorphology*, *121*(12), 55–68, doi:10.1016/j.geomorph.2009.02.010.

Duran, O., V. Schwammle, and H. Herrmann (2005), Breeding and solitary wave behavior of dunes, *Phys. Rev. E*, *72*(2), 021308, doi:10.1103/PhysRevE.72.021308.

Elliott, A. H., and N. H. Brooks (1997a), Transfer of nonsorbing solutes to a streambed with bed forms: Laboratory experiments, *Water Resour. Res.*, *33*(1), 137–151, doi:10.1029/96WR02783.

Elliott, A. H., and N. H. Brooks (1997b), Transfer of nonsorbing solutes to a streambed with bed forms: Theory, *Water Resour. Res.*, *33*(1), 123–136, doi:10.1029/96WR02784.

Endo, N., K. Taniguchi, and A. Katsuki (2004), Observation of the whole process of interaction between barchans by flume experiments, *Geophys. Res. Lett.*, *31*, L12503, doi:10.1029/2004GL020168.

Engelund, F., and J. Fredsoe (1982), Sediment ripples and dunes, *Annu. Rev. Fluid Mech.*, *14*(1), 13–37, doi:10.1146/annurev.fl.14.010182.000305.

Engelund, F., and E. Hansen (1967), *A Monograph on Sediment Transport in Alluvial Streams*, Teknisk Vorlag, Copenhagen, Denmark.

Ewing, R. C., and G. Kocurek (2010), Aeolian dune-field pattern boundary conditions, *Geomorphology*, *114*(3), 175–187, doi:10.1016/j.geomorph.2009.06.015.

Flemming, B. W. (2000), On the dimensional adjustment of subaqueous dunes in response to changing flow conditions: A conceptual process model, in Marine Sandwave Dynamics, Proceedings of an International Workshop Held in Lille, France, 23 and 24 March 2000, edited by A. Trentesaux, and T. Garlan, pp. 61–67, Univ. of Lille 1, Lille, France.

Fourriere, A., P. Claudin, and B. Andreotti (2010), Bed forms in a turbulent stream: Formation of ripples by primary linear instability and of dunes by nonlinear pattern coarsening, *J. Fluid Mech.*, *649*, 287–328, doi:10.1017/S0022112009993466.

Fredsoe, J. (1979), Unsteady flow in straight alluvial streams: Modification of individual dunes, *J. Fluid Mech.*, *91*(03), 497–512, doi:10.1017/S002211207900029X.

Fredsoe, J. (1982), Shape and dimensions of stationary dunes in rivers, *J. Hydraul. Div. Am. Soc. Civ. Eng.*, *108*(HY8), 932–947.

Frings, R. M., and M. G. Kleinhans (2008), Complex variations in sediment transport at three large river bifurcations during discharge waves in the river Rhine, *Sedimentology*, *55*(5), 1145–1171, doi:10.1111/j.1365-3091.2007.00940.x.

Fuhrboter, A. (1983), Zur Bildung von makroskopischen Ordnungstrukturen (Stromungsgriffel und Dunen) aus sehr kleinen Zufallsstorungen, *Mitteilungen des Leichtweiss-Instituts*, *79*, 1–51.

Gabel, S. L. (1993), Geometry and kinematics of dunes during steady and unsteady flows in the Calamus River, Nebr., USA, *Sedimentology*, *40*(2), 237–269, doi:10.1111/j.1365-3091.1993.tb01763.x.

Gee, D. M. (1975), Bed form response to nonsteady flows, *J. Hydraul. Div. Am. Soc. Civ. Eng.*, *101*(NHY3), 437–449.

Gilbert, G. (1914), The transportation of debris by running water, U.S. Geol. Surv. Prof. Pap. 86, U.S. Geol. Survey, Washington, D. C.

Gill, M. A. (1971), Height of sand dunes in open channel flows, *J. Hydraul. Div. Am. Soc. Civ. Eng.*, *97*(12), 2067–2074.

Grotzinger, J., et al. (2005), Stratigraphy and sedimentology of a dry to wet eolian depositional system, Burns Formation, Meridiani Planum, Mars, *Earth Planet. Sci. Lett.*, *240*(1), 11–72, doi:10.1016/j.epsl.2005.09.039.

Harvey, J. W., et al. (2012), Hydrogeomorphology of the hyporheic zone: Stream solute and fine particle interactions with a dynamic streambed, *J. Geophys. Res.*, *117*, G00N11, doi:10.1029/2012JG002043.

Huntley, D. A., G. Coco, K. R. Bryan, and A. B. Murray (2008), Influence of defects on sorted bed form dynamics, *Geophys. Res. Lett.*, *35*(2), L02601, doi:10.1029/2007GL030512.

Jerolmack, D. J., and D. Mohrig (2005a), Frozen dynamics of migrating bed forms, *Geology*, *33*(1), 57–60.

Jerolmack, D. J., and D. Mohrig (2005b), A unified model for subaqueous bed form dynamics, *Water Resour. Res.*, *41*(12), W12421, doi:10.1029/2005WR004329.

Jones, C. M. (1977), Effects of varying discharge regimes on bed form sedimentary structures in modern rivers, *Geology*, *5*(9), 567–570.

Jordan, P. R. (1965), Fluvial sediment of the Mississippi River at St. Louis, Missouri, *U.S. Geol. Surv. Water Supply Pap.* 1802, U.S. Geol. Survey, Washington, D. C.

Julien, P. Y., and G. J. Klaassen (1995), Sand-dune geometry of large rivers during floods, *J. Hydraul. Eng.*, *121*(9), 657–663.

Julien, P. Y., G. J. Klaassen, W. B. M. Ten Brinke, and A. W. E. Wilbers (2002), Case study: Bed resistance of Rhine River during 1998 flood, *J. Hydraul. Eng.*, *128*(12), 1042–1050.

Karim, F. (1995), Bed configuration and hydraulic resistance in alluvial-channel flows, *J. Hydraul. Eng.*, *121*(1), 15–25, doi:10.1061/(ASCE)0733-9429(1995)121:1(15).

Karim, F. (1999), Bed form geometry in sand-bed flows, *J. Hydraul. Eng.*, *125*(12), 1253–1261, doi:10.1061/(ASCE)0733-9429(1999)125:12(1253).

Katsuki, A., M. Kikuchi, and N. Endo (2005), Emergence of a barchan belt in a unidirectional flow: Experiment and numerical simulation, *J. Phys. Soc. Jpn.*, *74*(3), 878–881, doi:10.1143/JPSJ.74.878.

Kennedy, J. F. (1969), The formation of sediment ripples, dunes, and anti-dunes, *Annu. Rev. Fluid Mech.*, *1*(1), 147–168, doi:10.1146/annurev.fl.01.010169.001051.

Kocurek, G., and R. C. Ewing (2005), Aeolian dune field self-organization - implications for the formation of simple versus complex dune-field patterns, *Geomorphology*, *72*(1–4), 94–105, doi:10.1016/j.geomorph.2005.05.005.

Kocurek, G., R. C. Ewing, and D. Mohrig (2010), How do bed form patterns arise? New views on the role of bed form interactions within a set of boundary conditions, *Earth Surf. Processes Landforms*, *35*(1), 51–63, doi:10.1002/esp.1913.

Kostaschuk, R., and P. Villard (1996), Flow and sediment transport over large subaqueous dunes: Fraser River, Canada, *Sedimentology*, *43*(5), 849–863.

Lancaster, N. (1988), Controls of eolian dune size and spacing, *Geology*, *16*(11), 972–975.

Leclair, S. F. (2002), Preservation of cross-strata due to the migration of subaqueous dunes: An experimental investigation, *Sedimentology*, *49*(6), 1157–1180, doi:10.1046/j.1365-3091.2002.00482.x.

Leclair, S. F., and A. Blom (2005), A qualitative analysis of the distribution of bed-surface elevation and the characteristics of associated deposits for subaqueous dunes, *Spec. Publ. Int. Assoc. Sedimentol.*, *35*, 121–134.

Li, M. Z. (1994), Direct skin friction measurements and stress partitioning over movable sand ripples, *J. Geophys. Res.*, *99*(C1), 791–799, doi:10.1029/93JC02445.

McElroy, B., and D. Mohrig (2009), Nature of deformation of sandy bed forms, *J. Geophys. Res.*, *114*, F00A04, doi:10.1029/2008JF001220.

McLean, S. R. (1990), The stability of ripples and dunes, *Earth Sci. Rev.*, *29*, 131–144.

Neill, C. (1968), Bed forms in the lower red Deer River, Alberta, *J. Hydrol.*, *7*(1), 58–85, doi:10.1016/0022-1694(68)90195-9.

Nelson, J. M., B. L. Logan, P. J. Kinzel, Y. Shimizu, S. Giri, R. L. Shreve, and S. R. McLean (2011), Bed form response to flow variability, *Earth Surf. Processes Landforms*, *36*(14), 1938–1947, doi:10.1002/esp.2212.

Nikora, V. I., and D. M. Hicks (1997), Scaling relationships for sand wave development in unidirectional flow, *J. Hydraul. Eng.*, *123*(12), 1152–1156.

Nikora, V. I., A. N. Sukhodolov, and P. M. Rowinski (1997), Statistical sand wave dynamics in one-directional water flows, *J. Fluid Mech.*, *351*, 17–39.

Nino, Y., A. Atala, M. Barahona, and D. Aracena (2002), Discrete particle model for analyzing bed form development, *J. Hydraul. Eng.*, *128*(4), 381–389, doi:10.1061/(ASCE)0733-9429(2002)128:4(381).

Nittrouer, J. A., M. A. Allison, and R. Campanella (2008), Bed form transport rates for the lowermost Mississippi River, *J. Geophys. Res.*, *113*, F03004, doi:10.1029/2007JF000795.

Nittrouer, J. A., J. Shaw, M. P. Lamb, and D. Mohrig (2012), Spatial and temporal trends for water-flow velocity and bed-material sediment transport in the lower Mississippi River, *Geol. Soc. Am. Bull.*, *124*(3–4), 400–414, doi:10.1130/B30497.1.

Nordin, C. F. (1971), Statistical properties of dune profiles, *U.S. Geol. Surv. Prof. Pap. 562-F*, U.S. Geol. Survey, Washington, D. C.

Paarlberg, A. J., C. M. Dohmen-Janssen, S. J. M. H. Hulscher, and P. Termes (2009), Modeling river dune evolution using a parameterization of flow separation, *J. Geophys. Res.*, *114*, F01014, doi:10.1029/2007JF000910.

Paarlberg, A. J., C. M. Dohmen-Janssen, S. J. M. H. Hulscher, P. Termes, and R. Schielen (2010), Modelling the effect of time-dependent river dune evolution on bed roughness and stage, *Earth Surf. Processes Landforms*, *35*(15), 1854–1866, doi:10.1002/esp.2074.

Packman, A. I., and N. H. Brooks (2001), Hyporheic exchange of solutes and colloids with moving bed forms, *Water Resour. Res.*, *37*(10), 2591–2601, doi:10.1029/2001WR000477.

Packman, A. I., N. H. Brooks, and J. J. Morgan (2000), A physicochemical model for colloid exchange between a stream and a sand streambed with bed forms, *Water Resour. Res.*, *36*(8), 2351–2361, doi:10.1029/2000WR900059.

Paola, C., and L. Borgman (1991), Reconstructing random topography from preserved stratification, *Sedimentology*, *38*(4), 553–565.

Raudkivi, A. J. (2006), Transition from ripples to dunes, *J. Hydraul. Eng.*, *132*(12), 1316–1320, doi:10.1061/(ASCE)0733-9429(2006)132:12(1316).

Raudkivi, A. J., and H. Witte (1990), Development of bed features, *J. Hydraul. Eng.*, *116*(9), 1063–1079, doi:10.1061/(ASCE)0733-9429(1990)116:9(1063).

Robert, A., and W. Uhlman (2001), An experimental study on the ripple-dune transition, *Earth Surf. Processes Landforms*, *26*(6), 615–629, doi:10.1002/esp.211.

Rubin, D. M., and H. Ikeda (1990), Flume experiments on the alignment of transverse, oblique, and longitudinal dunes in directionally varying flows, *Sedimentology*, *37*(4), 673–684.

Rubin, D. M., and D. S. McCulloch (1980), Single and superimposed bed forms: A synthesis of San Francisco Bay and flume observations, *Sediment. Geol.*, *26*(1–3), 207–231, doi:10.1016/0037-0738(80)90012-3.

Schwammle, V., and H. J. Herrmann (2003), Geomorphology: Solitary wave behaviour of sand dunes, *Nature*, *426*(6967), 619–620, doi:10.1038/426619a.

Shimizu, Y., S. Giri, S. Yamaguchi, and J. Nelson (2009), Numerical simulation of dune-flat bed transition and stage-discharge relationship with hysteresis effect, *Water Resour. Res.*, *45*, W04429, doi:10.1029/2008WR006830.

Simons, D., and E. Richardson (1961), Forms of bed roughness in alluvial channels, *J. Hydraul. Div. Am. Soc. Civ. Eng.*, *87*(3), 87–105.

Simons, D., and E. Richardson (1962), Depth-discharge relations in alluvial channels, *J. Hydraul. Div. Am. Soc. Civ. Eng.*, *88*(5), 57–72.

Simons, D., E. Richardson, and C. Nordin (1965), Bedload equation for ripples and dunes, *U.S. Geol. Surv. Prof. Pap. 462-H*, U.S. Geol. Survey, Washington, D. C.

Southard, J. B. (1991), Experimental determination of bed form stability, *Annu. Rev. Earth Planet. Sci.*, *19*(1), 423–455, doi:10.1146/annurev.ea.19.050191.002231.

Stein, R. A. (1965), Laboratory studies of total load and apparent bed load, *J. Geophys. Res.*, *70*(8), 1831–1842, doi:10.1029/JZ070i008p01831.

Stonedahl, S. H., J. W. Harvey, A. Worman, M. Salehin, and A. I. Packman (2010), A multiscale model for integrating hyporheic exchange from ripples to meanders, *Water Resour. Res.*, *46*(12), W12539, doi:10.1029/2009WR008865.

Ten Brinke, W. B. M., A. W. E. Wilbers, and C. Wesseling (1999), Dune growth, decay and migration rates during a large-magnitude flood at a sand and mixed sand-gravel bed in the Dutch Rhine River system, *Spec. Publ. Int. Assoc. Sedimentol.*, *28*, 15–32, doi:10.1002/9781444304213.ch2.

Thibodeaux, L. J., and J. D. Boyle (1987), Bed form-generated convective transport in bottom sediment, *Nature*, *325*(6102), 341–343, doi:10.1038/325341a0.

Traykovski, P. (2007), Observations of wave orbital scale ripples and a non-equilibrium time-dependent model, *J. Geophys. Res.*, *112*(C6), C06026, doi:10.1029/2006JC003811.

van der Mark, C. F., and A. Blom (2007), A new and widely applicable tool for determining the geometric properties of bed forms, CE&M Research Report 2007R-003/WEM-002 ISSN 1568-4652, University of Twente, Enschede, Netherlands.

van der Mark, C. F., A. Blom, and S. J. M. H. Hulscher (2008), Quantification of variability in bed form geometry, *J. Geophys. Res.*, *113*, F03020, doi:10.1029/2007JF000940.

van Rijn, L. (1984), Sediment transport, Part III: Bed forms and alluvial roughness, *J. Hydraul. Eng.*, *110*(12), 1733–1754.

Vermeesch, P. (2011), Solitary wave behavior in sand dunes observed from space, *Geophys. Res. Lett.*, *38*, L22402, doi:10.1029/2011GL049610.

Warren, A., and D. Allison (1998), The palaeoenvironmental significance of dune size hierarchies, *Palaeogeogr. Palaeoclimatol. Palaeoecol.*, *137*(3–4), 289–303, doi:10.1016/S0031-0182(97)00110-7.

Werner, B. T., and G. Kocurek (1997), Bed form dynamics: Does the tail wag the dog?, *Geology*, *25*(9), 771–774.

Werner, B. T., and G. Kocurek (1999), Bed form spacing from defect dynamics, *Geology*, *27*(8), 727–730.

Wewetzer, S. F. K., and R. W. Duck (1999), Bed forms of the middle reaches of the Tay Estuary, Scotland, *Spec. Publ. Int. Assoc. Sedimentol.*, *28*, 33–41, doi:10.1002/9781444304213.ch3.

Wiberg, P. L., and J. M. Nelson (1992), Unidirectional flow over asymmetric and symmetric ripples, *J. Geophys. Res.*, *97*(C8), 12745–12761.

Wijbenga, J. H. A., and G. J. Klaassen (1983), Changes in bed form dimensions under unsteady flow conditions in a straight flume, *Spec. Publ. Int. Assoc. Sedimentol.*, *6*, 35–48.

Wijbenga, J. H. A., and A. R. Van Nes (1986), Flow resistance and bed form dimensions for varying flow conditions; results of flume experiments with flood waves, *TOW Rivers Rep. R 567-XXV/M 1314 part XIII, WL/Delft Hydraulics*, Delft, Netherlands.

Wilbers, A., and W. Ten Brinke (2003), The response of subaqueous dunes to floods in sand and gravel bed reaches of the Dutch Rhine, *Sedimentology*, *50*(6), 1013–1034, doi:10.1046/j.1365-3091.2003.00585.x.

Yalin, M. S. (1964), Geometrical properties of sand waves, *J. Hydraul. Div. Am. Soc. Civ. Eng.*, *90*(HY5), 105–119.

Yalin, M. S. (1992), *River Mechanics*, Pergamon, Oxford, U. K.